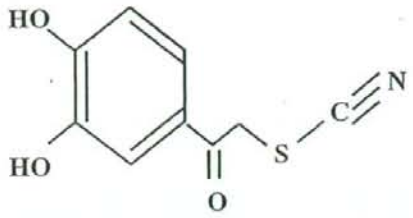

FIGURE 1. The structure of BIX (1-(3,4-dihydroxyphenyl)-2-thiocyanate-ethanone).

protein and sample buffer with 10% 2-mercaptoethanol was subjected to 10% sodium dodecyl sulfate-polyacrylamide gel electrophoresis. The separated protein was then transferred onto a polyvinylidene difluoride membrane (Immobilon-P; Millipore Corporation, Bedford, MA). For immunoblotting, the following primary antibodies were used: rabbit anti-CHOP polyclonal antibody (1:1000; Santa Cruz), mouse anti-β-actin monoclonal antibody (1:4000; Sigma-Aldrich), and rabbit anti-green fluorescent protein (GFP) polyclonal antibody (1:1000; Medical & Biological Laboratories Co. Ltd., Nagoya, Japan). The secondary antibody used was either goat anti-rabbit HRP-conjugated (1:2000) or goat anti-mouse HRP-conjugated (1:2000). The immunoreactive bands were visualized using a chemiluminescent substrate (SuperSignal West Femto Maximum Sensitivity Substrate; Pierce Biotechnology). The band intensity was measured using an imaging analyzer (Lumino Imaging Analyzer; Toyobo, Osaka, Japan) and a gel analysis electrophoresis analysis software (Gel Pro Analyzer; Media Cybernetics, Atlanta, GA).

Statistical Analysis

Data are presented as the means ± SE. Statistical comparisons were made by way of Dunnett's test or Student's *t*-test using statistical analysis software (STAT VIEW version 5.0; SAS Institute, Cary, NC). $P < 0.05$ was considered to indicate statistical significance.

RESULTS

BiP mRNA in RGC-5 Preferentially Induced by BIX

To clarify whether BIX (Fig. 1) induces BiP in RGC-5, we used semi-quantitative RT-PCR and real-time PCR, using a specific primer and a TaqMan probe recognizing BiP mRNA, respectively. Real-time PCR revealed that the level of BiP mRNA was significantly elevated at 0.5 to 12 h (peak at approximately 6 h) after treatment with 50 μM BIX (Fig. 2A). At 6 h after treatment with BIX (2 to 150 μM), BiP mRNA was increased concentration-dependently (Fig. 2B). Next, we used real-time *PCR* to investigate whether BIX might affect the expressions of any other genes related to the ER stress response, such as GRP94, calreticulin, protein kinase inhibitor of 58 kDa ($p58^{IPK}$), or asparagine synthetase (ASNS; Fig. 2C). Real-time PCR revealed significant inductions of ASNS and calreticulin mRNAs at 6 h after treatment with BIX at 2 and 10 μM, respectively. At 50 μM, BIX induced the mRNAs for GRP94 at 12 h, calreticulin at 6 and 12 h, $p58^{IPK}$ at 6 h, and ASNS at 12 h. In contrast, GRP94 mRNA was significantly reduced at 4 h after treatment with 50 μM BIX.

Protective Effect of BIX against ER Stress–Induced Cell Death in RGC-5 Cells

To investigate whether BIX can prevent the cell death induced by ER stress, RGC-5 cells were pretreated for 12 h with or without BIX, then treated with 2 μg/mL tunicamycin, and finally incubated for a further 48 h. Fluorescence micrographs of Hoechst 33342 and PI staining revealed 38.4 ± 4.5% cell death ($n = 8$) at 48 h after tunicamycin treatment, (control: 0.9 ± 0.2%, $n = 8$), and pretreatment with BIX at 1 and 5 μM significantly reduced this cell death (Figs. 3A, 3B). Next, we evaluated the expression of CHOP protein after tunicamycin treatment. There was no CHOP protein expression in either nontreated or BIX-treated cells (Figs. 3C, 3D). On the other

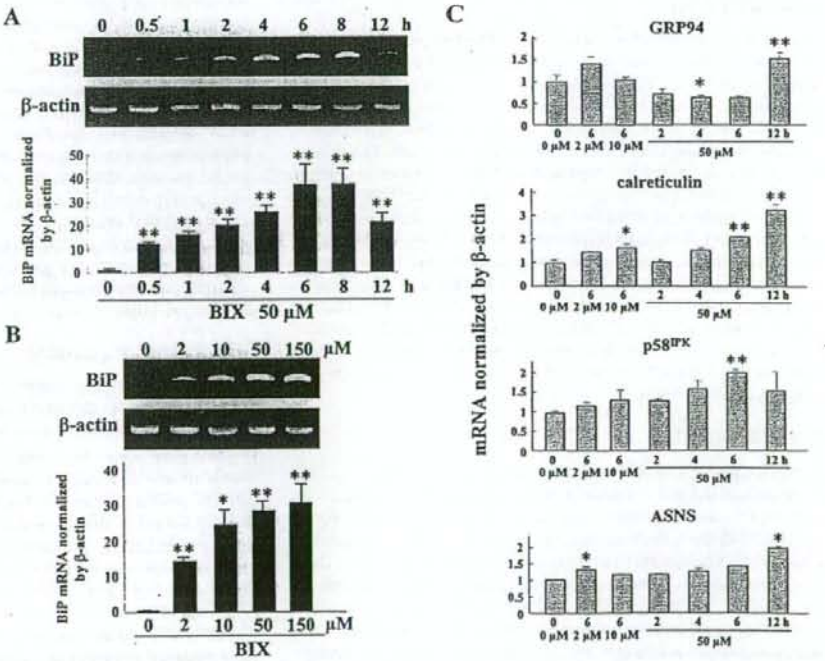

FIGURE 2. Effect of BIX on BiP mRNA expression BIX in RGC-5 cells. (A) Time-dependent induction of BiP mRNA after treatment with 50 μM BIX and (B) concentration-dependence of BIX-induced BiP mRNA expression are each shown by semi-quantitative RT-PCR (*upper panel*) and real-time PCR (*lower panel*). β-Actin mRNA is shown as an internal control. (C) Induction of GRP94, calreticulin, $p58^{IPK}$, and ASNS mRNAs at 6 h after treatment with 2 or 10 μM BIX and at 2 to 12 h after treatment with 50 μM BIX. Data are shown as mean ± SE ($n = 3$ or 4). $^*P < 0.05$, $^{**}P < 0.01$ versus 0 μM (A and B) or 0 μM/0 h (C).

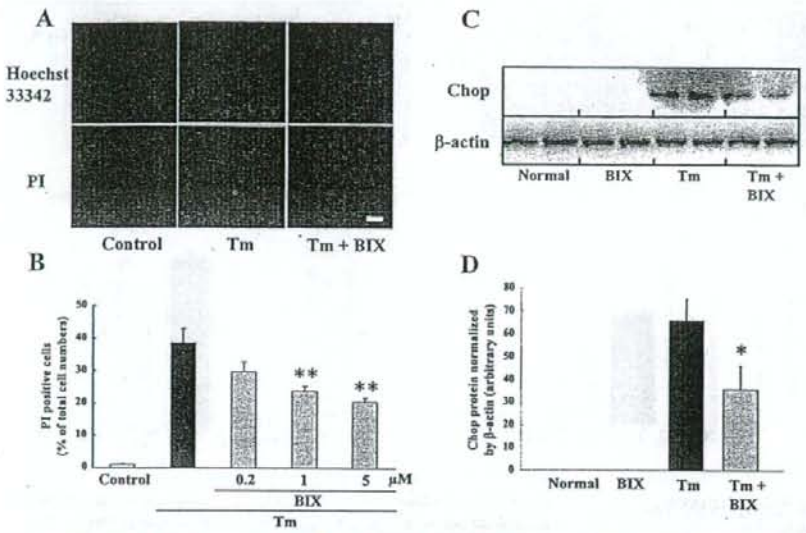

FIGURE 3. Effects of BIX on tunicamycin-induced cell death and CHOP protein expression in RGC-5 cells. (A) RGC-5 cells were pretreated with vehicle or with 1 μM BIX for 12 h, and then immersed in fresh medium (control) or in medium supplemented with 2 μg/mL tunicamycin (Tm; labeled Tm or Tm + BIX). *Upper* photomicrographs show Hoechst 33342 and *lower* ones propidium iodide (PI) staining at 48 h after tunicamycin stimulation. Scale bar represents 25 μm. (B) Numbers of PI-positive cells after tunicamycin treatment. Pretreatment of cells with BIX (1 and 5 μM) significantly reduced the amount of cell death (vs. cells treated with tunicamycin alone). (C) Immunoblot of CHOP protein shows that tunicamycin induced significant CHOP expression, and that pretreatment of cells with BIX at 5 μM reduced this expression with no change in the level of β-actin. *Upper panel* shows CHOP and *lower panel* shows β-actin. (D) Quantitative representations of β-actin-based tunicamycin-induced CHOP protein expression (in arbitrary units). Data are shown as mean ± SE ($n = 6$ or 8). $^*P < 0.05$, $^{**}P < 0.01$ versus tunicamycin alone.

hand, tunicamycin markedly induced CHOP protein, while pretreatment with BIX at 5 μM reduced this expression to almost half the value seen after tunicamycin treatment alone (Figs. 3C, 3D).

Effects of BIX on Cell Damage Induced by Staurosporine in RGC-5 Culture

To investigate whether BIX protects non-ER stress-induced cell death, we examined staurosporine-induced cell death. Staurosporine at 30 nM for 24 h reduced cell viability to approximately 60% of control (Fig. 4). There was no statistical difference between BIX (1 and 5 μM)-treated and vehicle-treated group.

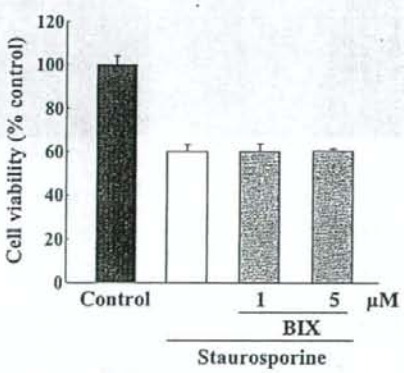

FIGURE 4. Effect of BIX on the cell death induced by staurosporine in RGC-5. RGC-5 cells were pretreated with vehicle or with BIX (1 or 5 μM) for 12 h, and then immersed in fresh medium (control) or in medium supplemented with staurosporine at 30 nM. At the end of this culture period, cell death was assessed by WST-8 assay (Cell Counting Kit-8; Dojin Kagaku). Data are shown as mean ± SE ($n = 6$).

BiP Protein in the Mouse Retina Induced by Intravitreous Injection of BIX

Compared with that in the nontreated retina, BiP protein expression in GCL and IPL was significantly increased at 6 and 12 h after intravitreal injection of BIX (5 nmol; Figs. 5A, 5B). Optical density analysis confirmed that administration of BIX induced BiP protein in vivo (Fig. 5D).

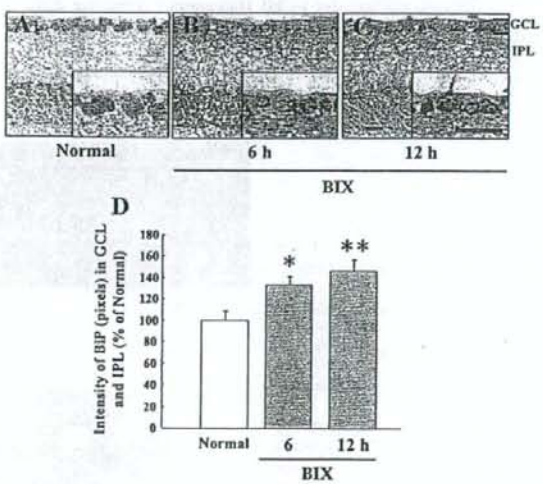

FIGURE 5. BiP protein expression in the mouse retina induced by intravitreous injection of BIX. Immunostaining probed with an antibody against BiP/GRP78. (A) Nontreated, (B) 6 h, and (C) 12 h after intravitreous injection of BIX (5 nmol). (D) Expression ratio for BiP induction intravitreous injection of BIX is represented as the ratio of intensity values. Data are shown as mean ± SE ($n = 6$). $^*P < 0.05$, $^{**}P < 0.01$ versus nontreated normal retina. Each scale bar represents 25 μm.

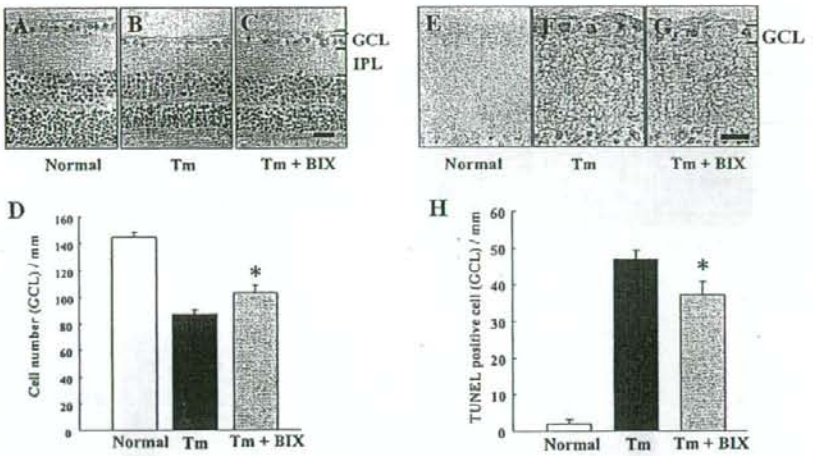

FIGURE 6. Effects of BIX on retinal damage induced by intravitreal injection of tunicamycin in mice. Hematoxylin and eosin staining of cross-sections of (A) nontreated, (B) Tm-treated, and (C) Tm plus BIX-treated mouse retinas at seven days after intravitreal injection of tunicamycin (1 μg) either alone or with BIX (5 nmol). (D) Damage was evaluated by counting cell numbers in GCL at seven days after the above injections. TUNEL staining of cross-sections of (E) nontreated, (F) Tm-treated, and (G) Tm plus BIX-treated mouse retinas at seven days after the above injections. (H) Effect of BIX on Tm-induced expression of TUNEL-positive cells at 24 h after the above injections. Data are shown as mean ± SE ($n = 9$ or 10). *$P < 0.05$ versus tunicamycin alone. Scale bars each represent 25 μm.

Protective Effect of BIX against Tunicamycin-Induced Retinal Damage in Mice

Tunicamycin decreased the cell number in GCL at 7 days after its intravitreal injection (vs. nontreated retinas; Figs. 6A, 6B). There was significantly less cell loss in GCL when BIX (5 nmol) was co-administered with the tunicamycin (Figs. 6B–6D). In addition, intravitreal injection of tunicamycin increased the number of TUNEL-positive cells in GCL at 24 h (vs. nontreated retinas; Figs. 6E, 6F). BIX (5 nmol), when co-administered with the tunicamycin, significantly reduced the number of TUNEL-positive cells (vs. tunicamycin alone; Figs. 6F–6H).

Protective Effect of BIX against Tunicamycin-Induced Retinal Damage in Thy-1-CFP Transgenic Mice

In this experiment on Thy-1-CFP transgenic mice, we confirmed the effect of BIX in a larger retinal area than that evaluated in Figure 6D. We counted the number of Thy-1-CFP-positive cells (in flatmounts) in the four white areas shown 1 mm from the center of the optic disc in Figure 7E, and then totaled these values. In the Thy-1-CFP–transgenic mouse retina, axonal fibers were evenly and densely distributed. There were congested CFP-positive cells in the vehicle-treated retina (Fig. 7A), and no change was observed in BIX-treated retinas without tunicamycin treatment (Fig. 7B). Intravitreal injection of tunicamycin decreased the Thy-1-CFP–positive cell count at 7 days (vs. vehicle-treated retina; Figs. 7A, 7C). BIX at 5 nmol, when co-administered with the tunicamycin, significantly inhibited this cell loss (Figs. 7C, 7D, 7F).

Effect of BIX on Tunicamycin-Induced CHOP Expression in Mice

Representative photograph of a nontreated retina is shown in Figure 8A. No change was observed in the BIX-treated retina (Fig. 8B). Optical density analysis of CHOP protein immunoreactivity in GCL and IPL showed that intravitreal injection of tunicamycin (1 μg) significantly increased the level of CHOP protein at 72 h after the injection (Fig. 8C). BIX (5 nmol), when co-administered with the tunicamycin, significantly inhibited this effect (Figs. 8D, 8E).

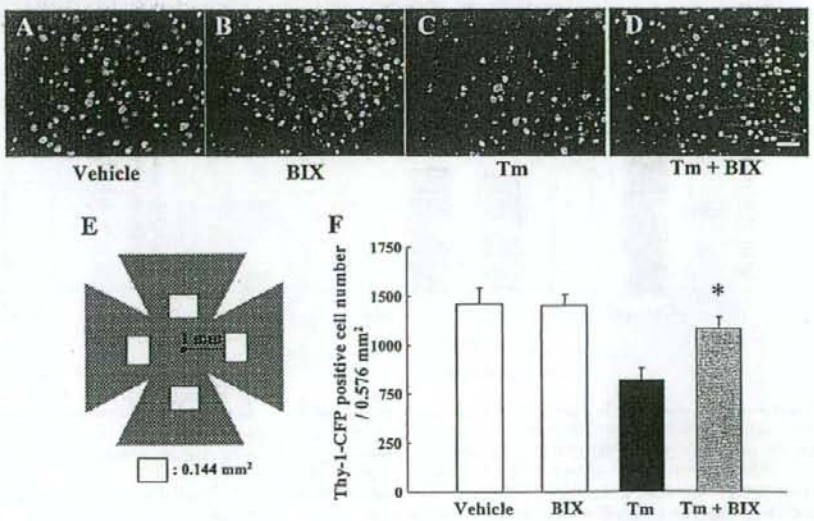

FIGURE 7. Effects of BIX on retinal damage induced by intravitreal injection of tunicamycin in Thy-1-CFP transgenic mice. Mouse retinas (flatmounts) at seven days after intravitreal injection of (A) vehicle, (B) BIX (5 nmol), (C) Tm (1 μg), or (D) Tm (1 μg) plus BIX (5 nmol). Damage was evaluated by counting Thy-1-CFP-positive cell numbers in the four *white* areas shown in (E) (each area 0.144 mm² × 4 areas; total 0.576 mm²) at seven days after the above intravitreal injections. (F) Effect of BIX against Tm-induced damage (indicated by decreased number of Thy-1-CFP-positive cells) at seven days after intravitreal injection. Data are shown as mean ± SE ($n = 9$ or 10). *$P < 0.05$ versus tunicamycin alone. Scale bar represents 25 μm.

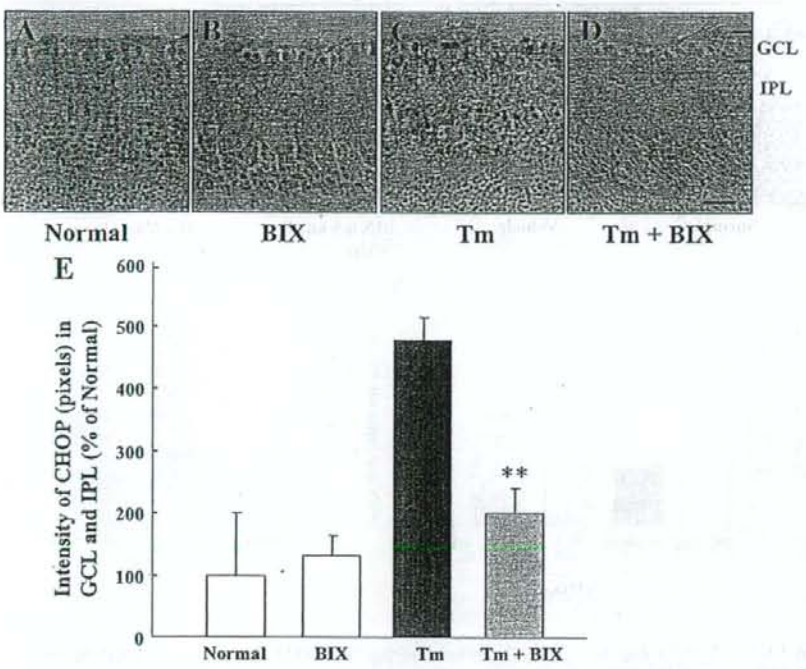

FIGURE 8. Effect of BIX on tunicamycin-induced CHOP expression in the mouse retina. Mouse retinas (cross-sections) either (A) nontreated or at three days after intravitreal injection of (B) BIX (5 nmol), (C) Tm (1 μg) or (D) Tm (1 μg) plus BIX (5 nmol). (E) Relative density of CHOP protein expression in GCL and IPL at three days after the above intravitreal injections. Data are shown as mean ± SE ($n = 6$). $^{**}P < 0.01$ versus tunicamycin alone. Scale bar represents 25 μm.

Effect of BIX on Tunicamycin-Induced XBP-1 Expression in ERAI Mice

In ERAI mice, the fluorescence intensity arising from the XBP-1–venus fusion protein (indicating ER stress activation) can be easily visualized, allowing evaluation of the effect of ER stress on the retina. In the representative photographs of flatmount retinas from ERAI mice shown in Figure 9, no difference was observed between vehicle-treated and BIX-treated retinas (Fig. 9B). Intravitreal injection of tunicamycin (1 μg) induced XBP-1–venus expression (vs. the vehicle-treated retina; Fig. 9C). Immunoblot analysis of XBP-1–venus protein expression in the retina (using an anti-GFP antibody) showed that intravitreal injection of tunicamycin (1 μg) significantly raised the level of XBP-1–venus protein, and that BIX (5 nmol), when co-administered with the tunicamycin (Fig. 9D), significantly inhibited this effect (Figs. 9E, 9F).

Protective Effect of BIX against NMDA-Induced Retinal Damage in Mice

A representative photograph of a nontreated retina is shown in Figure 10A. Intravitreal injection of NMDA (a) decreased the

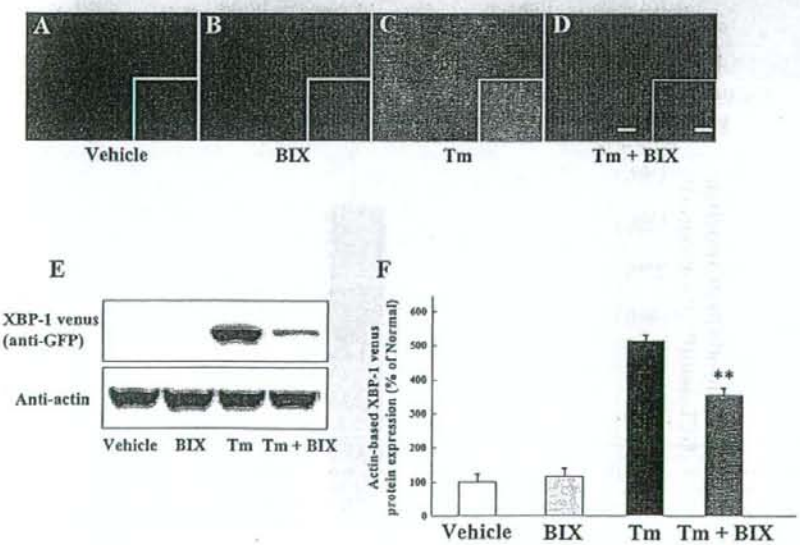

FIGURE 9. Effect of BIX on tunicamycin-induced XBP-1 venus expression in ERAI mice. Mouse retinas (flatmounts) at 24 h after intravitreal injection of (A) vehicle, (B) BIX (5 nmol), (C) Tm (1 μg) or (D) Tm (1 μg) plus BIX (5 nmol). (E) *Upper panel* shows XBP-1 venus protein expression, while *lower panel* shows β-actin protein expression at 24 h after the above injections. (F) Western blot analysis showing effect of BIX on Tm-induced expression of β-actin-based XBP-1 venus protein expression at 24 h after the above injections. Data are shown as mean ± SE ($n = 8$). $^{*}P < 0.01$ versus tunicamycin alone. Scale bars in main photomicrographs and in *insets* represent 25 and 5 μm, respectively.

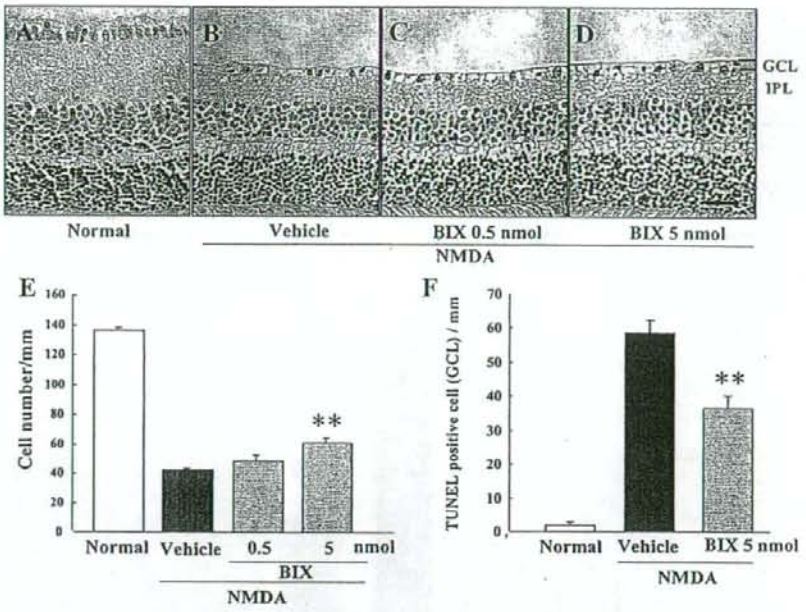

FIGURE 10. Effects of BIX on retinal damage induced by intravitreal injection of NMDA in mice. Mouse retinas (cross-sections) either (A) nontreated or at seven days after intravitreal injection of (B) NMDA (40 nmol) alone or (C, D) NMDA (40 nmol) plus BIX (0.5 or 5 nmol). (E) Damage was evaluated by counting cell numbers in GCL at seven days after the above intravitreal injections. (F) Effect of BIX on NMDA-induced expression of TUNEL-positive cells at 24 h after intravitreal injection of NMDA (40 nmol) either alone or with BIX (5 nmol). Data are shown as mean ± SE ($n = 9$ or 10). $^{**}P < 0.01$ versus NMDA-treated control group. Scale bar represents 25 μm.

cell number in GCL at 7 days (Figs. 10B, 10E) and (b) increased the number of TUNEL-positive cells in GCL at 24 h (vs. nontreated normal retina; Fig. 10F). BIX (5 nmol), when co-administered with the NMDA, significantly reduced (vs. NMDA alone) both the cell loss in GCL (Figs. 10D, 10E) and the number of TUNEL-positive cells (Fig. 10F). On the other hand, there was no statistical difference between BIX (0.5 nmol)- and vehicle-treated group in NMDA-induced cell death in GCL (Figs. 10C, 10E).

Effect of BIX on NMDA-Induced CHOP Expression in Mice

A representative photograph of a nontreated retina is shown in Figure 11A and no change was detected between nontreated

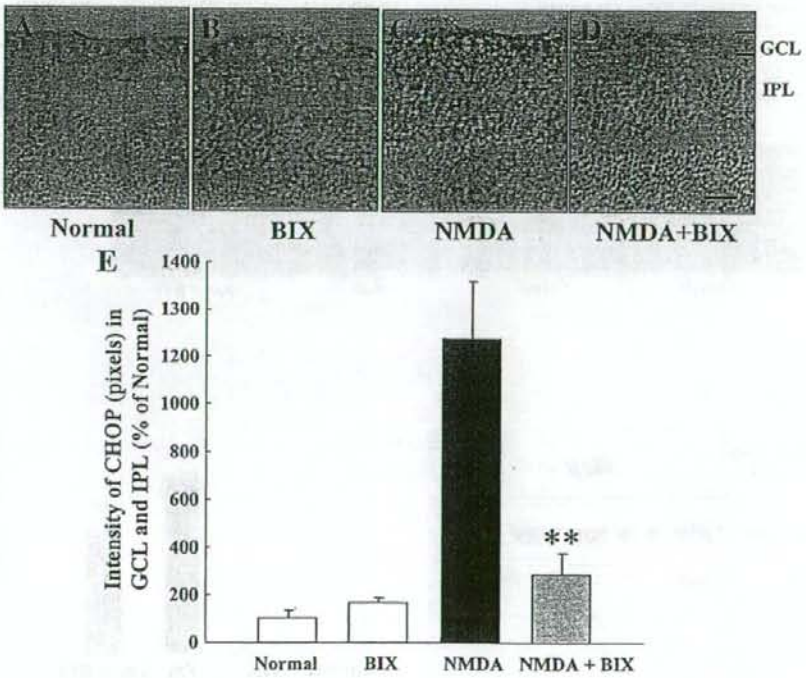

FIGURE 11. Effect of BIX on NMDA-induced CHOP expression in mice. Mouse retinas (cross-sections) either (A) nontreated or at three days after intravitreal injection of (B) NMDA (40 nmol) alone or (C) NMDA (40 nmol), or (D) NMDA (40 nmol) plus BIX (5 nmol). (E) Relative density of CHOP protein expression in GCL and IPL at three days after the above intravitreal injections. Data are shown as mean ± SE ($n = 6$). $^{**}P < 0.01$ versus NMDA alone. Scale bar represents 25 μm.

retina and the BIX-treated retina without NMDA treatment (Figs. 11A, 11B). Optical density analysis of CHOP protein immunoreactivity in GCL and IPL showed that intravitreal injection of NMDA (40 nmol) significantly increased the level of CHOP protein at 72 h after the injection (Fig. 11C). When co-administered with the NMDA, BIX (5 nmol) significantly inhibited this effect (Figs. 11D, 11E).

Discussion

In the present study, we confirmed that BIX preferentially induces BiP mRNA in RGC-5. Although it also induced GRP94, calreticulin, $p58^{IPK}$, and ASNS, these inductions were lower than that of BiP. This is consistent with our previous study that BIX preferentially induced BiP with slight inductions of GRP94, calreticulin, and CHOP mediated by the activating transcription factor 6 (ATF6) pathway accompanied by activation of ERSEs, and that BIX does not affect the pathway downstream of IRE1 or the translational control branch downstream of PERK in SK-N-SH cells.[32] Therefore, BIX is not just an ER stressor such as tunicamycin or thapsigargin, and we consider that the induction of BiP by BIX is mediated by the ATF6 pathway in RGC-5 similar to that in SK-N-SH cells. Next, we evaluated the effects of BIX, as a preferential inducer of BiP, on ER stress–induced in vitro cell death in RGC-5 (a rat ganglion cell-line) and in vivo retinal damage in mice. We found that BIX reduced tunicamycin-induced cell death in RGC-5 and also reduced both tunicamycin-induced and NMDA-induced retinal damage in mice. Our previous study revealed that BIX (a) reduced tunicamycin-induced cell death in SK-N-SH cells, (b) contributed to the induction of BiP expression via the ATF-6 pathway (but not via the PERK or IRE1 pathways), and (c) on intracerebroventricular injection, prevented the neuronal damage induced by focal ischemia in mice.[32] Furthermore, immunostaining revealed that intravitreal injection of BIX significantly induced BiP protein in mouse retina. Particularly, it expressed in GCL and IPL (versus both the normal and the sham retina). On the other hand, there was little protective effect of BIX against RGC-5 damages after staurosporine treatment. Staurosporine is well known as a nonspecific inhibitor of protein kinases and initiates caspase-dependent apoptosis in many cell types.[41,42] Our previous studies revealed that staurosporine induced cell death without any changes in the expression of BiP or CHOP protein.[12,43] Furthermore, preliminary study showed that treatment with BIX (1 and 5 μM) did not inhibit RGC-5 cell death 48 h after serum deprivation, which does not induce any UPR-responses such as BiP or CHOP (unpublished data). These results strongly support that BIX selectively protects cell damage induced by ER stress.

Recently, we reported that in mice, increased expressions of XBP-1 splicing, BiP, and CHOP could be detected after the induction of retinal damage by tunicamycin, NMDA, or an elevation of intraocular pressure.[13] That report was the first to demonstrate an involvement of ER stress and BiP in retinal cell death in mice. Hence, in the present study we asked whether BIX can prevent such retinal damage. By histologic analysis and TUNEL staining, we estimated that BIX reduced tunicamycin-induced retinal damage in GCL. However, the cell counts in partial cross sections provide a comparatively small sample on which quantitative morphometry can be used to judge such an effect. Therefore, we used Thy-1-CFP transgenic mice[36] to examine the effect of BIX in a large retinal area. This transgene contains a CFP gene under the direction of regulatory elements derived from the mouse Thy-1 gene, and the transgenic mice express CFP protein in RGC and in the inner part of the IPL of the retina.[36] Our results show that BIX exerted a protective effect against tunicamycin-induced retinal damage in the Thy-1-CFP transgenic mouse. However, it is possible that microglial cells become co-labeled with CFP by phagocytosis of the dying RGCs. In this study, we evaluated CFP-positive cells in 7 days after tunicamycin injection. In our previous and preliminary studies, activated microglia cells in GCL were increased at 3 days after NMDA injection[13] and their increases were almost ceased within the 7 days (unpublished data). Furthermore, microglial cells can be distinguished with neuronal cells by their morphologic features.[44] In fact, microglial cells were scarcely observed at seven days after tunicamycin injection, similar to that at seven days after NMDA injection. When we investigated the effect of BIX on NMDA-induced retinal damage in ddY mice, we found that it significantly attenuated such damage. NMDA is well known to induce RGC death and optic-nerve loss (effects mediated by excitatory glutamate receptor), and such neuronal death is believed to play a role in many neurologic and neurodegenerative diseases.[45,46] Recently, Uehara et al.[47] noted that mild exposure to NMDA induced apoptotic cell death in primary cortical culture, and they demonstrated this effect to be caused by an accumulation of polyubiquitinated proteins and increases in XBP-1 mRNA splicing and CHOP mRNA (reflecting activation of the UPR signaling pathway). They also found that protein-disulphide isomerase, which assists in the maturation and transport of unfolded secretory proteins, prevented the neurotoxicity associated with ER stress. These findings suggested that activation of ER stress may participate in the retinal cell death occurring after NMDA-receptor activation and/or an ischemic insult.[47]

In our investigation of the mechanisms underlying the above-mentioned effects, we focused on CHOP. Since CHOP is a member of the CCAAT/enhancer-binding protein family that is induced by ER stress and participates in ER-mediated apoptosis, CHOP may be a key molecule in retinal cell death.[48] We found that treatment with tunicamycin induced apoptotic cell death in RGC-5 and also induced a production of ER stress–related proteins (BiP, the phosphorylated form of eIF2α, and CHOP protein). BIX reduced both the cell death and the CHOP protein expression induced by tunicamycin in RGC-5 in vitro. BIX also attenuated the CHOP protein expression induced by either tunicamycin or NMDA in the mouse retina in vivo. As mentioned above, BIX may affect CHOP protein expression through ATF6 pathway, but no change was observed in BIX-treated RGC-5. In our previous data in SK-N-SH cells, BIX slightly increased CHOP mRNA only at 2 h after the treatment. Expression of CHOP is mainly regulated by three transcription factors—ATF4, cleaved ATF6, and x-box binding protein-1 (XBP-1)—which are downstream effectors during ER stress in similar to other ER chaperones. These differences between BiP and CHOP expression by BIX may be due to the difference of their promoters. CHOP promoter contains at least two ERSE motifs (CHOP ERSE-1 and CHOP ERSE-2) located in opposite directions with a 9 bp overlap, and one of ERSEs is inactive.[49] On the other hand, BiP promoter has three functional ERSE motifs of the rat GRP78 promoter (ERSE-163, ERSE-131, and ERSE-98).[50] These variations in each promoter may contribute to the differences among the expressions of ER chaperons induced by BIX and the lack of CHOP expression.

Subsequently, we monitored XBP-1 activation in the mouse retina in vivo, using ERAI transgenic mice.[37] Effective identification of cells under ER stress conditions is possible in the retina in these mice, as described in our previous report.[13] Here, ERAI mice carrying the F-XBP1ΔDBD-venus expression gene were used to monitor ER stress. The fluorescence intensity arising from the X-box binding protein (XBP1)-venus fusion protein, indicating ER stress activation, was increased in cells within GCL and IPL at 24 h after injection of tunicamycin into the vitreous. BIX significantly reduced this expression, indicating that BIX may attenuate the retinal damage induced

by ER stress-associated factors. In our previous study,[32] we found that BIX induced BiP protein expression via the ATF-6 pathway (not via other ER stress-associated factors such as the PERK and IRE1 pathways) in SK-N-SH cells. Possibly, the protective mechanism underlying the effect of BIX on the mouse retina may be the same as that revealed by our previous study, but further experiments will be needed to clarify this issue.

In conclusion, we have demonstrated that BIX, a preferential inducer of BiP, inhibits both the neuronal cell death induced by ER stress in vitro in RGC-5 cells and in vivo in the mouse retina. Hence, an increase in BiP might be one of the targets of mechanisms bestowing neuroprotection in retinal diseases.

Acknowledgments

The authors thank Masayuki Miura (Department of Genetics, Graduate School of Pharmaceutical Sciences, University of Tokyo, Tokyo, Japan) for the kind gift of ERAI mice, and Rumi Uchibayashi and Shunsake Imai for technical assistance.

References

1. Travers KJ, Patil CK, Wodicka L, Lockhart DJ, Weissman JS, Walter P. Functional and genomic analyses reveal an essential coordination between the unfolded protein response and ER-associated degradation. *Cell.* 2000;101:249–258.
2. Harding HP, Novoa I, Zhang Y, et al. Regulated translation initiation controls stress-induced gene expression in mammalian cells. *Mol Cell.* 2000;6:1099–1108.
3. Schroder M, Kaufman RJ. The mammalian unfolded protein response. *Annu Rev Biochem.* 2005;74:739–789.
4. Katayama T, Imaizumi K, Honda A, et al. Disturbed activation of endoplasmic reticulum stress transducers by familial Alzheimer's disease-linked presenilin-1 mutations. *J Biol Chem.* 2001;276:43446–43454.
5. Ryu EJ, Harding HP, Angelastro JM, Vitolo OV, Ron D, Greene LA. Endoplasmic reticulum stress and the unfolded protein response in cellular models of Parkinson's disease. *J Neurosci.* 2002;22:10690–10698.
6. Oyadomari S, Koizumi A, Takeda K, et al. Targeted disruption of the Chop gene delays endoplasmic reticulum stress-mediated diabetes. *J Clin Invest.* 2002;109:525–532.
7. Roybal CN, Yang S, Sun CW, et al. Homocysteine increases the expression of vascular endothelial growth factor by a mechanism involving endoplasmic reticulum stress and transcription factor ATF4. *J Biol Chem.* 2004;279:14844–14852.
8. Rebello G, Ramesar R, Vorster A, et al. Apoptosis-inducing signal sequence mutation in carbonic anhydrase IV identified in patients with the RP17 form of retinitis pigmentosa. *Proc Natl Acad Sci USA.* 2004;101:6617–6622.
9. Lin JH, Li H, Yasumura D, et al. IRE1 signaling affects cell fate during the unfolded protein response. *Science.* 2007;318:944–949.
10. Joe MK, Sohn S, Hur W, Moon Y, Choi YR, Kee C. Accumulation of mutant myocilins in ER leads to ER stress and potential cytotoxicity in human trabecular meshwork cells. *Biochem Biophys Res Commun.* 2003;312:592–600.
11. Gould DB, Marchant JK, Savinova OV, Smith RS, John SW. Col4a1 mutation causes endoplasmic reticulum stress and genetically modifiable ocular dysgenesis. *Hum Mol Genet.* 2007;16:798–807.
12. Shimazawa M, Ito Y, Inokuchi Y, Hara H. Involvement of double-stranded RNA-dependent protein kinase in ER stress-induced retinal neuron damage. *Invest Ophthalmol Vis Sci.* 2007;48:3729–3736.
13. Shimazawa M, Inokuchi Y, Ito Y, et al. Involvement of ER stress in retinal cell death. *Mol Vis.* 2007;13:578–587.
14. Mahoney WC, Duksin D. Biological activities of the two major components of tunicamycin. *J Biol Chem.* 1979;254:6572–6576.
15. Awai M, Koga T, Inomata Y, et al. NMDA-induced retinal injury is mediated by an endoplasmic reticulum stress-related protein, CHOP/GADD153. *J Neurochem.* 2006;96:43–52.
16. Lee YK, Brewer JW, Hellman R, Hendershot LM. BiP and immunoglobulin light chain cooperate to control the folding of heavy chain and ensure the fidelity of immunoglobulin assembly. *Mol Biol Cell.* 1999;10:2209–2219.
17. Li WW, Alexandre S, Cao X, Lee AS. Transactivation of the grp78 promoter by Ca^{2+} depletion. A comparative analysis with A23187 and the endoplasmic reticulum Ca^{2+}-ATPase inhibitor thapsigargin. *J Biol Chem.* 1993;268:12003–12009.
18. van de Put FH, Elliott AC. The endoplasmic reticulum can act as a functional Ca^{2+} store in all subcellular regions of the pancreatic acinar cell. *J Biol Chem.* 1997;272:27764–27770.
19. Lievremont JP, Rizzuto R, Hendershot L, Meldolesi J. BiP, a major chaperone protein of the endoplasmic reticulum lumen, plays a direct and important role in the storage of the rapidly exchanging pool of Ca^{2+}. *J Biol Chem.* 1997;272:30873–30879.
20. Helenius A. How N-linked oligosaccharides affect glycoprotein folding in the endoplasmic reticulum. *Mol Biol Cell.* 1994;5:253–265.
21. Kuznetsov G, Chen LB, Nigam SK. Multiple molecular chaperones complex with misfolded large oligomeric glycoproteins in the endoplasmic reticulum. *J Biol Chem.* 1997;272:3057–3063.
22. Klausner RD, Sitia R. Protein degradation in the endoplasmic reticulum. *Cell.* 1990;62:611–614.
23. Blond-Elguindi S, Cwirla SE, Dower WJ, et al. Affinity panning of a library of peptides displayed on bacteriophages reveals the binding specificity of BiP. *Cell.* 1993;75:717–728.
24. Knarr G, Gething MJ, Modrow S, Buchner J. BiP binding sequences in antibodies. *J Biol Chem.* 1995;270:27589–27594.
25. Knarr G, Modrow S, Todd A, Gething MJ, Buchner J. BiP-binding sequences in HIV gp160. Implications for the binding specificity of bip. *J Biol Chem.* 1999;274:29850–29857.
26. Brodsky JL, Werner ED, Dubas ME, Goeckeler JL, Kruse KB, McCracken AA. The requirement for molecular chaperones during endoplasmic reticulum-associated protein degradation demonstrates that protein export and import are mechanistically distinct. *J Biol Chem.* 1999;274:3453–3460.
27. Meerovitch K, Wing S, Goltzman D. Proparathyroid hormone-related protein is associated with the chaperone protein BiP and undergoes proteasome-mediated degradation. *J Biol Chem.* 1998;273:21025–21030.
28. Katayama T, Imaizumi K, Sato N, et al. Presenilin-1 mutations downregulate the signalling pathway of the unfolded-protein response. *Nat Cell Biol.* 1999;1:479–485.
29. Yu Z, Luo H, Fu W, Mattson MP. The endoplasmic reticulum stress-responsive protein GRP78 protects neurons against excitotoxicity and apoptosis: suppression of oxidative stress and stabilization of calcium homeostasis. *Exp Neurol.* 1999;155:302–314.
30. Rao RV, Peel A, Logvinova A, et al. Coupling endoplasmic reticulum stress to the cell death program: role of the ER chaperone GRP78. *FEBS Lett.* 2002;514:122–128.
31. Reddy RK, Mao C, Baumeister P, Austin RC, Kaufman RJ, Lee AS. Endoplasmic reticulum chaperone protein GRP78 protects cells from apoptosis induced by topoisomerase inhibitors: role of ATP binding site in suppression of caspase-7 activation. *J Biol Chem.* 2003;278:20915–20924.
32. Kudo T, Kanemoto S, Hara H, et al. A molecular chaperone inducer protects neurons from ER stress. *Cell Death Differ.* 2008;15:364–375.
33. Krishnamoorthy RR, Agarwal P, Prasanna G, et al. Characterization of a transformed rat retinal ganglion cell line. *Brain Res Mol Brain Res.* 2001;86:1–12.
34. Chen D, Padiernos E, Ding F, Lossos IS, Lopez CD. Apoptosis-stimulating protein of p53-2 (ASPP2/53BP2L) is an E2F target gene. *Cell Death Differ.* 2005;12:358–368.
35. Jiang Y, Ahn EY, Ryu SH, et al. Cytotoxicity of psammaplin A from a two-sponge association may correlate with the inhibition of DNA replication. *BMC Cancer.* 2004;4:70.
36. Feng G, Mellor RH, Bernstein M, et al. Imaging neuronal subsets in transgenic mice expressing multiple spectral variants of GFP. *Neuron.* 2000;28:41–51.
37. Iwawaki T, Akai R, Kohno K, Miura M. A transgenic mouse model for monitoring endoplasmic reticulum stress. *Nat Med.* 2004;10:98–102.

38. Siliprandi R, Canella R, Carmignoto G, et al. N-methyl-D-aspartate-induced neurotoxicity in the adult rat retina. *Vis Neurosci.* 1992; 8:567–573.
39. Jeon CJ, Strettoi E, Masland RH. The major cell populations of the mouse retina. *J Neurosci.* 1998;18:8936–8946.
40. Onozuka T, Sawamura D, Goto M, Yokota K, Shimizu H. Possible role of endoplasmic reticulum stress in the pathogenesis of Darier's disease. *J Dermatol Sci.* 2006;41:217–220.
41. Weil M, Jacobson MD, Coles HS, et al. Constitutive expression of the machinery for programmed cell death. *J Cell Biol.* 1996;133: 1053–1059.
42. Taylor J, Gatchalian CL, Keen G, Rubin LL. Apoptosis in cerebellar granule neurones: involvement of interleukin-1 beta converting enzyme-like proteases. *J Neurochem.* 1997;68:1598–1605.
43. Inokuchi Y, Shimazawa M, Nakajima Y, Suemori S, Mishima S, Hara H. Brazilian green propolis protects against retinal damage in vitro and in vivo. *Evid Based Complement Alternat Med.* 2006;3:71–77.
44. Chidlow G, Wood JP, Manavis J, Osborne NN, Casson RJ. Expression of osteopontin in the rat retina: effects of excitotoxic and ischemic injuries. *Invest Ophthalmol Vis Sci.* 2008;49:762–771.
45. Sucher NJ, Lipton SA, Dreyer EB. Molecular basis of glutamate toxicity in retinal ganglion cells. *Vision Res.* 1997;37:3483–3493.
46. Henneberry RC, Novelli A, Cox JA, Lysko PG. Neurotoxicity at the N-methyl-D-aspartate receptor in energy-compromised neurons. An hypothesis for cell death in aging and disease. *Ann NY Acad Sci.* 1989;568:225–233.
47. Uehara T, Nakamura T, Yao D, et al. S-nitrosylated protein-disulphide isomerase links protein misfolding to neurodegeneration. *Nature.* 2006;441:513–517.
48. Wang XZ, Lawson B, Brewer JW, et al. Signals from the stressed endoplasmic reticulum induce C/EBP-homologous protein (CHOP/GADD153). *Mol Cell Biol.* 1996;16:4273–4280.
49. Ubeda M, Habener JF. CHOP gene expression in response to endoplasmic-reticular stress requires NFY interaction with different domains of a conserved DNA-binding element. *Nucleic Acids Res.* 2000;28:4987–4997.
50. Foti DM, Welihinda A, Kaufman RJ, Lee AS. Conservation and divergence of the yeast and mammalian unfolded protein response. Activation of specific mammalian endoplasmic reticulum stress element of the grp78/BiP promoter by yeast Hac1. *J Biol Chem.* 1999;274:30402–30409.

Neuroscience 159 (2009) 760–769

THALIDOMIDE PROTECTS AGAINST ISCHEMIC NEURONAL DAMAGE INDUCED BY FOCAL CEREBRAL ISCHEMIA IN MICE

K. HYAKKOKU,[a] Y. NAKAJIMA,[a] H. IZUTA,[a] M. SHIMAZAWA,[a] T. YAMAMOTO,[b] N. SHIBATA[b] AND H. HARA[a]*

[a]*Department of Biofunctional Evaluation, Molecular Pharmacology, Gifu Pharmaceutical University, 5-6-1 Mitahora-higashi, Gifu 502-8585, Japan*

[b]*Department of Applied Chemistry, Nagoya Institute of Technology, Gokisocho Shouwa-ku, Nagoya 466-8555, Japan*

Abstract—We aimed to examine whether thalidomide might inhibit the neuronal damage resulting from focal cerebral ischemia, and if so to explore the neuroprotective mechanism. Focal cerebral ischemia was induced by permanent middle cerebral artery occlusion (MCAO) in mice, and thalidomide was intraperitoneally administered a total of three times (at 10 min before, just before, and 1 h after MCAO). Thalidomide significantly reduced (a) the infarct area and volume at 24 and 72 h after MCAO and (b) the neurological score at 72 h after MCAO. Brains were also histochemically assessed for apoptosis and lipid peroxidation using terminal deoxynucleotidyl transferase-mediated dUTP nick end-labeling (TUNEL) staining and an antibody recognizing 8-hydroxy-2′-deoxyguanosine (8-OHdG), respectively. Thalidomide reduced both the number of TUNEL-positive cells and the oxidative damage. However, post-treatment of thalidomide [20 mg/kg, three times (at just after, 1 h after, 3 h after MCAO)] did not reduce the infarct volume. In an *in vitro* study, we examined the effects of thalidomide on lipid peroxidation in mouse brain homogenates and on the production of various radical species. Thalidomide inhibited both the lipid peroxidation and the production of H_2O_2 and $O_2 \cdot^-$ (but not HO^-) radicals. We also measured the brain concentration of TNF-α by ELISA. The TNF-α level in the brain was significantly increased at 9–24 h after MCAO. However, thalidomide did not reduce the elevated TNF-α level at either 12 or 24 h after MCAO. These findings indicate that thalidomide has neuroprotective effects against ischemic neuronal damage in mice, and that an inhibitory action of thalidomide against oxidative stress may be partly responsible for these neuroprotective effects.

Key words: focal cerebral ischemia, middle cerebral artery occlusion, oxidative stress, thalidomide, TNF-α.

Stroke is the third most common cause of death after heart attack and cancer, and it has profound negative social and economic effects. The current treatment for complete stroke is only partially successful at reversing neurodegeneration and restoring premorbid function. Clinical and experimental data suggest that ischemic neuronal damage is at least partly caused by the free-radicals production and lipid peroxidation that occurs either during the ischemia itself or following reperfusion (Flamm et al., 1978; Hara et al., 1993; Toyoda et al., 2004). Ischemia causes an imbalance between antioxidants and oxygen radicals, with an accumulations of toxic free radicals increasing the susceptibility of brain tissues to oxidative damage via inflammation, apoptosis, lipid peroxidation of membranes, and DNA oxidation (Chan et al., 2001). Hence, one of the prime goals of neuroprotective strategies is to reduce oxidative damage, and indeed edaravone, a radical scavenger, has been an approved neuroprotective agent for the treatment of acute cerebral infarction since 2001 in Japan.

Thalidomide [α-(N-phthalimido)-glutarimide] was first released in Europe and Canada as a rapidly acting and hangover-free sedative in 1956. Reports of phocomelia in the infants born to women who had taken thalidomide during pregnancy started to surface a few years later, leading to its withdrawal from the market. Despite its teratogenicity, thalidomide was approved by the United States Food and Drug Administration in 1998 as a treatment for erythema nodosum leprosum. The clinical efficacy of thalidomide against inflammatory and autoimmune diseases is attributed in part to its ability to inhibit TNF-α production (Sampaio et al., 1991; Moreira et al., 1993; Klausner et al., 1996). It has been reported that thalidomide reduces ischemic injury of the spinal cord in rabbits (Lee et al., 2007), and that it decreases polymorphonuclear leukocyte infiltration, retinal edema, and the synthesis of vascular endothelial growth factor (VEGF) and TNF-α following ischemia/reperfusion injury to the guinea-pig retina (Aydogan et al., 2007).

TNF-α, a cytokine involved in systemic inflammation, is a member of a group of cytokines that all stimulate the acute phase reaction. TNF causes apoptotic cell death, cellular proliferation, inflammation, and tumorigenesis. At 6 and 22 h after middle cerebral artery occlusion (MCAO), activated spleen cells are major secretors of TNF-α and some other cytokines (Offner et al., 2006). This response is associated with marked proinflammatory changes in the brain. Thus, the neuroimmune axis appears to have a feedback loop in which focal cerebral ischemia results in widespread activation of inflammatory cytokines in peripheral immune organs, and this in turn modulates CNS pathophysiology.

Given the background described above, we performed the present study to examine the neuroprotective effects of

*Corresponding author. Tel: +81-58-237-8596; fax: +81-58-237-8596.
E-mail address: hidehara@gifu-pu.ac.jp (H. Hara).

Abbreviations: DCFH, nonfluorescent di-chlorofluorescein; DMSO, dimethyl sulfoxide; DPPH, diphenyl-*p*-picrylhydrazyl; ESR, electron spin resonance; MABP, mean arterial blood pressure; MCAO, middle cerebral artery occlusion; PBS, phosphate-buffered saline; rCBF, regional cerebral blood flow; RGC-5, Retinal ganglion cells; ROS, reactive oxygen species; TBA, thiobarbituric acid; TTC, 2,3,5-triphenyltetrazolium chloride; TUNEL, terminal deoxynucleotidyl transferase-mediated dUTP nick end-labeling; VEGF, vascular endothelial growth factor; 8-OHdG, 8-hydroxy-2′-deoxyguanosine.

0306-4522/09
doi:10.1016/j.neuroscience.2008.12.043

thalidomide against infarction, neurological deficits, and apoptosis in a murine focal cerebral ischemia model. In addition, we studied the mechanism of action of thalidomide, focusing on the extent to which ischemia induced TNF-α production in the ischemic brain (by ELISA) and oxidative stress [by assessing (i) radical-scavenging capacity in neuronal cells, (ii) immunohistochemical changes using 8-hydroxy-2′-deoxyguanosine (8-OHdG), (iii) lipid peroxidation in mouse brain homogenates using an assay for thiobarbituric acid (TBA) reactive substance, (iv) diphenyl-*p*-picrylhydrazyl (DPPH)-induced free radicals by electron spin resonance (ESR)-spin trapping and absorbance determinations].

EXPERIMENTAL PROCEDURES

Animals

The experimental designs and all procedures were in accordance with the U.S. National Institutes of Health Guide for the Care and Use of Laboratory Animals and the Animal Care Guidelines issued by the Animal Experimental Committee of Gifu Pharmaceutical University. All efforts were made to minimize both suffering and the number of animals used. All *in vivo* experiments were performed using male ddY mice (4 weeks old; body weight 22–28 g; Japan SLC Ltd., Shizuoka, Japan). The animals were housed at 24±2 °C under a 12-h light/dark cycle (lights on from 07:00–19:00 h). Each animal was used for one experiment only.

Drugs

Thalidomide was synthesized at the Department of Materials Engineering (Prof. N. Shibata), Nagoya Institute of Technology (Nagoya, Japan). 2,3,5-Triphenyltetrazolium chloride (TTC), sodium pentobarbital, and isoflurane were purchased from Sigma-Aldrich Co. (St. Louis, MO, USA), Nissan Kagaku (Tokyo, Japan), and Merck Hoei Ltd. (Osaka, Japan), respectively. DPPH and dimethyl sulfoxide (DMSO) were purchased from Sigma-Aldrich and Koso Chemical (Tokyo, Japan), respectively.

Focal cerebral ischemia model in mice

Anesthesia was induced using 2.0–3.0% isoflurane and maintained using 1.0–1.5% isoflurane (both in 70% N_2O/30% O_2) by means of an animal general anesthesia machine (Soft Lander; Sin-ei Industry Co. Ltd., Saitama, Japan). Body temperature was maintained at 37.0–37.5 °C with the aid of a heating pad and heating lamp. After a midline skin incision, the left external carotid artery was exposed, and its branches were occluded (Hara et al., 1996, 1997). An 8–0 nylon monofilament (Ethicon, Somerville, NJ, USA) coated with a mixture of silicone resin (Xantopren; Bayer Dental, Osaka, Japan) was introduced into the left internal carotid artery through the common carotid artery so as to occlude the origin of the middle cerebral artery. Then, the left common carotid artery was occluded. After the surgery, the mice were kept in the preoperative condition (room temperature; 24±2 °C) until sampling.

Thalidomide treatment

Thalidomide or DMSO 0.8 ml/kg (vehicle) was administered intraperitoneally (10, 20 and 50 mg/kg in DMSO) a total of three times (at 10 min before, just after, and 1 h after MCAO, or at just after, 1 h after, and 3 h after MCAO).

Physiological monitoring

A polyethylene catheter inserted into the left femoral artery was used to measure arterial blood pressure (MABP) and heart rate (Power Laboratory/8SP; AD Instrument, Osaka, Japan) 20 min before and 30 min after MCAO. Blood samples (50 μl) were taken before and at 30 min after the onset of ischemia for pH, pCO_2, and pO_2 being measured (i-STAT 300F; Abbott Co., Abbott Park, IL, USA). Regional cerebral blood flow (rCBF) was monitored by Doppler flowmetry (Omegaflow flo-N1; Omegawave Inc., Tokyo, Japan). A flexible probe was fixed to the skull (2 mm posterior and 6 mm lateral to bregma).

Assessment of cerebral infarction

To analyze infarct volume, mice were euthanized using sodium pentobarbital at 24 h or 72 h after MCAO, and forebrains were sectioned coronally into five slices (2 mm thick). These were placed in 2% TTC at 37 °C for 30 min. The infarcted areas and volumes were recorded as images using a digital camera (Coolpix 4500; Nikon, Tokyo, Japan), then quantified using an Image J (http://rsb.info.nih.gov/ij/download/) and calculated as in a previous report (Hara et al., 1997).

Neurological deficits

Mice were tested for neurological deficits at 72 h after MCAO. Scoring was done as described in our previous study (Hara et al., 1996), using the following scale: 0, no observable neurological deficits (normal); 1, failure to extend the right forepaw (mild); 2, circling to the contralateral side (moderate); 3, loss of walking or righting reflex (severe). The investigator (K.H.) who rated the mice was masked as to the group to which each mouse belonged.

Terminal deoxynucleotidyl transferase-mediated dUTP nick end-labeling (TUNEL) staining

The TUNEL assay was performed according to the manufacturer's instructions (Roche Molecular Biochemicals Inc., Mannheim, Germany). Ischemic areas of cortical brain sections 0.4–1.0 mm anterior to bregma (through the anterior commissure) were excised and used. For the identification of brain structures, we referred to a mouse brain atlas (Paxinos and Franklin, 2001). The brains were removed, fixed overnight in 4% paraformaldehyde, and immersed for 1 day in 25% sucrose with PBS. The brains were then embedded in a supporting medium for frozen-tissue specimens (OCT compound; Tissue-Tek). Cerebral sections 10 μm thick were cut on a cryostat at −25 °C, and stored at −80 °C until staining. After twice washing with phosphate-buffered saline (PBS), sections were incubated with terminal deoxyribonucleotidyl transferase (TdT) enzyme at 37 °C for 1 h. The sections were washed three times in PBS for 1 min at room temperature. Sections were subsequently incubated with an anti-fluorescein antibody–peroxidase conjugate at room temperature in a humidified chamber for 30 min, and then developed using DAB tetrahydrochloride peroxidase substrate.

Immunohistochemistry for 8-OHdG

Twenty-four hours after MCAO, mice were perfusion-fixed using heparinized saline followed by 4% paraformaldehyde in PBS, and the forebrain was processed and paraffin-embedded. After deparaffinization, sections were microwaved for 10 min at 121 °C in 10 μmol/l citric acid (pH 6.0), then allowed to cool to room temperature for 60 min. Sections were rinsed three times in PBS, incubated in 3% H_2O_2 in methanol for 30 min, then placed in PBS and blocked with 1% mouse serum for 30 min. A monoclonal antibody against 8-OHdG was applied to sections overnight at 4 °C. Secondary antibody (M.O.M. biotinylated anti-mouse) was applied for 10 min. The avidin/biotinylated horseradish peroxidase complex (ABC Elite kit; Vector Laboratories, UK) was applied for 30 min, and the sections were allowed to develop chromogen in 3,3-diaminobenzidine+nickel solution (Sigma-Aldrich) for 2 min. Ischemic areas of cortical brain sections 0.4–1.0 mm anterior to

Table 1. Physiological parameters measured 10 min before and 30 min after MCAO in vehicle group and thalidomide group

Parameters	Vehicle		Thalidomide	
	Before	During	Before	During
MABP (mm Hg)	63±3.7	72±3.3	66±5.6	74±3.5
Heart rate (per min)	403±15	390±14	421±29	442±31
pH	7.34±0.01	7.35±0.01	7.35±0.02	7.33±0.03
Arterial pCO_2 (mm Hg)	27±5.4	28±4.5	31.6±3.7	30±0.7
Arterial pO_2 (mm Hg)	184±8.0	204±4.3	168±12	158±12.3
rCBF (ml/min per 100 g)	73.8±8.1	18.1±2.5	71.2±5.9	17.1±7.2
% of before	100	24.5±3.7	100	24.0±8.6

None of the parameters analyzed was significantly different among the groups. Indicated values are expressed as mean±S.E., n=3.

bregma (through the anterior commissure) were excised and used. Therefore, in the present study, we cut coronal sections through the infarction (bregma 0.5 mm).

Cell counting

To quantify the number of DNA-fragmented cells present after MCAO, the numbers of TUNEL-positive cells in the caudate-putamen (as the ischemic core) and cortex (as the ischemic penumbra; two areas) were counted in a high-power field (×200) on a section through the anterior commissure by a masked investigator (K.H.). Each count was expressed as number/mm^2 (n=6 or 7).

Measurement of brain TNF-α

Twenty-four hours after MCAO, brains of mice were removed and the infarcted area cut out. Then, these tissues were centrifuged at 10,000 rpm for 20 min. After that, the supernatant fluid was removed and preserved at −80 °C. Then, the brain contents of TNF-α were measured by ELISA according to the kit instructions provided by R&D Systems (Minneapolis, MN, USA) for the Quantikine Mouse TNF-α/TNFSF1A, immunoassay. The sensitivity of this assay is ~5.1 pg/ml.

RGC-5 culture

Retinal ganglion cells (RGC-5) were presented by Dr. Agarwal (Department of Pathology and Anatomy, UNT Health Science Center, Fort Worth, TX, USA). RGC-5 were maintained in DMEM containing 10% FBS, 100 U/ml penicillin (Meiji Seika Kaisha Ltd., Tokyo, Japan), and 100 μg/ml streptomycin (Meiji Seika Kaisha Ltd.) under a humidified atmosphere of 95% air and 5% CO_2 at 37 °C. The cells were passaged by trypsinization every 3–4 days, as described in a previous report (Krishnamoorthy et al., 2001).

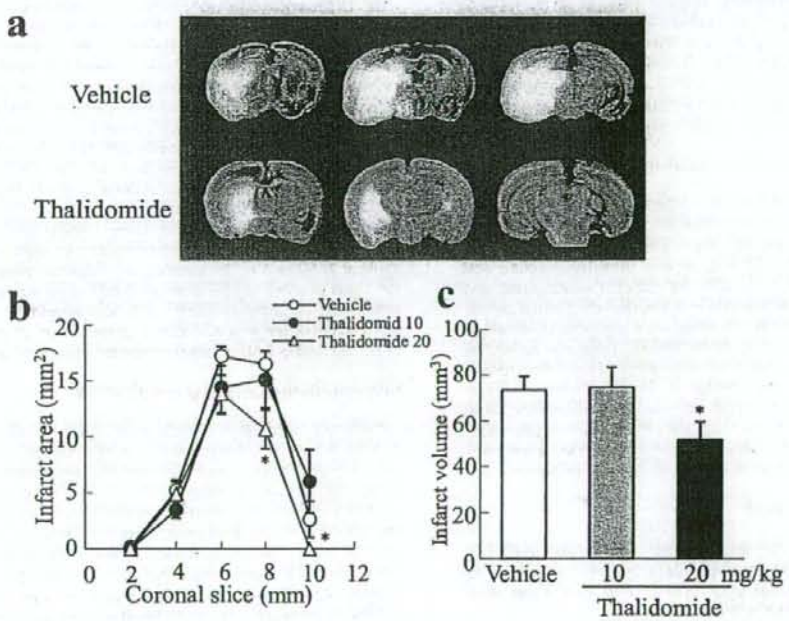

Fig. 1. Effects of thalidomide on infarction at 24 h after MCAO in mice. (a) TTC staining of coronal brain sections (2 mm thick) at 24 h after permanent MCAO in representative mice. Upper panels, vehicle-injected (control) mice. Lower panels, thalidomide (20 mg/kg, i.p., given three times)-treated mice. (b) Brain infarct area measured at 24 h after MCA occlusion. Brains were removed and the forebrains sliced into five coronal 2-mm sections. * P<0.05, vs. vehicle, n=8–15. (c) Effects of thalidomide on infarct volume (measured at 24 h after MCAO). * P<0.05 vs. vehicle, n=8–15.

Radical scavenging-capacity assay

This assay was measured in RGC-5 cellular radical. CM-H_2DCFDA was converted with DCFH by being taken into the cell and being cut with the intracellular enzyme (esterase). Radical species (H_2O_2, $O_2'^-$, and HO') oxidize nonfluorescent di-chlorofluorescein (DCFH) to fluorescent di-chlorofluorescein (DCF). Experiments were performed in D-MEM medium at 37 °C (Adom and Liu, 2005). To examine the antioxidant effects of thalidomide against radical species (H_2O_2, $O_2'^-$, and HO'), RGC-5 cells were seeded at 2×10^3 cells per well into 96-well plates. After incubating for 1 day, cells were washed by 1% FBS in D-MEM. We exchanged the cell culture medium to new D-MEM containing 1% FBS with thalidomide or vehicle for 1 h. The cellular radical probe CM-H_2DCFDA was added for 20 min and cells were washed with 1% FBS D-MEM with thalidomide or vehicle. Fluorescence was measured after adding reactive oxygen species (ROS)-generating compounds for various time-periods using excitation/emission wavelengths of 485/535 nm (Skan It RE for Varioskan Flash 2.4; Thermo Fisher Scientific, Waltham, MA, USA). H_2O_2 radicals were generated by treatment with H_2O_2 at 100 μM, $O_2'^-$ radicals were generated following treatment with KO_2 at 100 μM, and HO'radicals generated by treatment with H_2O_2 at 1 mM plus Fe perchlorate (II) at 100 μM. Radical integral was calculated by integrating the area under the CM-H_2DCFDA fluorescence intensity curve for 20 min after ROS-generating compounds treatment. Results represent the averages±S.E. of four independent experiments, with each treatment performed in duplicate.

ESR-spin trapping determinations of DPPH-induced free radical

The stable free radical, DPPH, was dissolved in ethanol (200 μM). The DPPH solution (250 μl) and a sample solution (250 μl) were mixed, and DPPH radical was measured after 90 s. The sample was dissolved in a mixture of ethanol and DMSO (9:1). The concentrations of DPPH radical were calculated from the double integrals of DPPH radical spectra (the areas of the DPPH radical spectra). The measurement conditions for ESR (JES-FA200; JEOL Ltd., Tokyo, Japan) were as follows: field sweep 305.0–335.0 mT; field modulation frequency, 100 kHz; field modulation width, 0.10 mT; amplitude, 500; sweep time, 4 min; time constant, 0.3 s; microwave power, 4 mW.

DPPH-induced free radicals

Free radical-scavenging activity was determined by the method of Mellors and Tappel (1966), which involved adding 0.125 ml of thalidomide or trolox solution (in DMSO) to 0.75 ml of ethanolic DPPH. The resulting decrease in DPPH absorption at 517 nm was measured after 30 min.

Lipid peroxidation in mouse forebrain homogenate

The supernatant fraction of a forebrain homogenate obtained from male adult ddY mice was prepared as described elsewhere (Hara and Kogure, 1990). Brain tissues were homogenized in a glass–

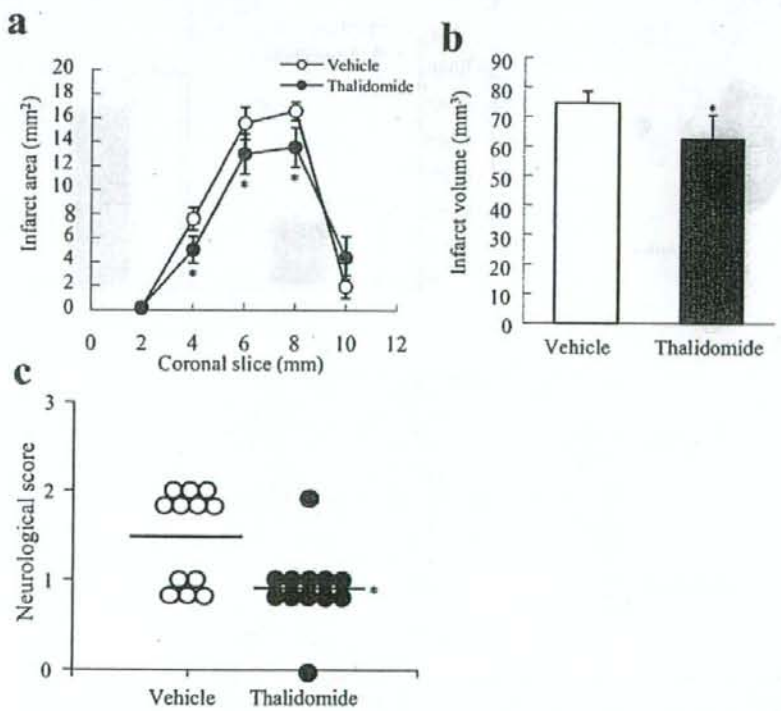

Fig. 2. Effects of thalidomide on infarction at 72 h after MCAO in mice. (a) Brain infarct area measured at 72 h after MCAO. Brains were removed and the forebrains sliced into five coronal 2-mm sections. * $P<0.05$ vs. vehicle, $n=12$–14. (b) Effects of thalidomide on infarct volume (measured at 72 h after MCAO). * $P<0.05$ vs. vehicle, $n=12$–14. (c) Effects of thalidomide on neurological deficits (assessed at 72 h after MCAO). * $P<0.05$ vs. Vehicle, $n=12$.

Teflon homogenizer in 4 vols. of ice-cold phosphate-saline buffer (50 mM, pH 7.4), and the homogenate was stored at −80 °C. The stock brain homogenate was diluted 10-fold with the same buffer, then 2 ml portions of the diluted homogenate were added to 10 μl of the test compound and incubated at 37 °C for 30 min. The reaction was stopped by adding 400 μl of 35% $HClO_4$, followed by centrifugation at 2800 rpm for 10 min. The supernatant (1 ml) was heated with 0.5 ml of TBA solution (5 g/l in 50% acetic acid) for 15 min at 100 °C. Absorbance was then measured at 532 nm.

Statistical analysis

All data are presented as means±S.E. Statistical comparisons were made using a one- or two-way analysis of variance followed by Student's *t*-test or Dunnett's test. Stat View software version 5.0 (SAS Institute Inc., Cary, NC, USA) was used. * $P<0.05$ was considered statistically significant.

RESULTS

Physiological parameters

There were no significant differences in MABP or heart rate, in arterial pH, pCO_2, or pO_2, or in rCBF between the vehicle- and thalidomide-treated groups (Table 1). Surface rCBF was reduced to approximately 25% of the baseline value immediately after MCAO in all mice (Table 1).

Infarction and neurological deficits

Twenty-four hours after MCAO, mice developed infarcts affecting the cortex and striatum. Thalidomide at 20 mg/kg, i.p., but not at 10 or 50 mg/kg, i.p. (given three times: namely, at 10 min before, just after, and 1 h after MCAO) decreased infarct area and volume at 24 h after MCA occlusion (Fig. 1a–c). Furthermore, at 20 mg/kg thalidomide significantly reduced infarct area, infarct volume, and neurological deficits at 72 h after MCAO (Fig. 2a–c). On the other hand, there was no significant change in infarct volume in post-treatment (at just after, 1 h after, and 3 h after MCAO) (vehicle; 73.5±5.9 mm^3, $n=15$ vs. thalidomide; 69.7±8.3 mm^3, $n=13$). In regional analysis, thalidomide at 20 mg/kg, i.p. reduced both infarct area and infarct volume in the cortex and the subcortex (data not shown).

Histological observation

The morphological features of TUNEL-stained cells are shown in Fig. 3. TUNEL-positive cells (exhibiting shrunken cell bodies and condensed nuclei) were distributed in the ischemic penumbra (Fig. 3a–A) and core (Fig. 3a–B) in the MCA territory. Thalidomide at 20 mg/kg, i.p. (given three

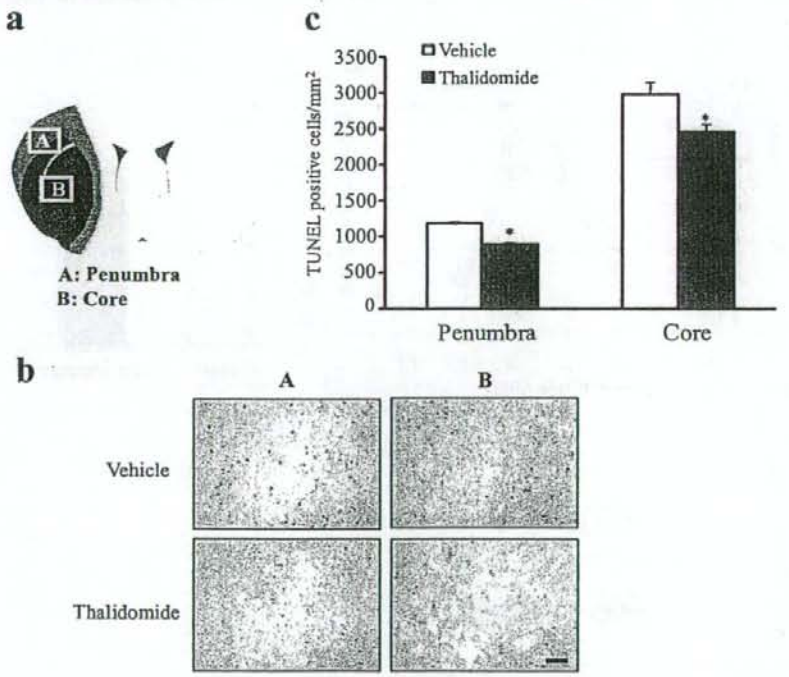

Fig. 3. Effect of thalidomide on TUNEL staining at 24 h after MCAO in mice. (a) Schematic drawing showing brain regions at 0.4–1.0 mm anterior to bregma (through the anterior commissure): (A, B) measurement areas in ischemic penumbra and ischemic core, respectively. The number of TUNEL-positive cells was counted in each of these areas, the average of the numbers obtained in the various sections for area A or B being taken as the number for the ischemic penumbra area or ischemic core area, respectively. (b) Thalidomide at 20 mg/kg, i.p. (given three times) reduced the number of TUNEL-positive cells (vs. Vehicle treatment) in both the ischemic penumbra and the ischemic core. Scale bar=25 μm. (c) Quantitative representation of TUNEL-positive cells in ischemic penumbra and core areas in mice treated with thalidomide or vehicle (see above). * $P<0.05$ vs. Vehicle, $n=5$.

times) significantly reduced the number of TUNEL-positive cells in both the ischemic penumbra and core (Fig. 3).

TNF-α concentration in MCAO-induced ischemic brain (by ELISA)

We first tested whether MCAO treatment increased the concentration of TNF-α in the ischemic brain. A significant increase in TNF-α concentration was detected as early as 9 h after MCAO. Then, we tested whether thalidomide at 20 mg/kg, i.p. (given three times) would decrease the MCAO-induced effect. We found no significant differences between the vehicle and thalidomide groups at either 12 or 24 h after MCAO (Fig. 4).

Effects of thalidomide on intracellular oxidation

To investigate the effects of thalidomide on the production of hydrogen peroxide (H_2O_2 radical), superoxide anion ($O_2 \cdot ^-$), and hydroxyl radical (· OH), we employed a radical scavenging-capacity assay using the ROS-sensitive probes CM-H_2DCFDA and APF. The kinetics of ROS reactivity (monitored as fluorescence generation) are shown in Fig. 5 (a, c, and e), with quantification in Fig. 5 (b, d, and f). H_2O_2 radicals were generated by treatment with H_2O_2 at 1 mM, and thalidomide at 0.1–10 μM scavenged the H_2O_2 radical (Fig. 5b). $O_2 \cdot ^-$ radicals were generated following treatment with KO_2 at 1 mM, and thalidomide at 1 and 10 μM scavenged the $O_2 \cdot ^-$ radical in a concentration-dependent manner (Fig. 5d). In contrast, the · OH radicals generated by treatment with H_2O_2 at 1 mM plus Fe perchlorate (II) at 100 μM were not scavenged by thalidomide at 0.1 to10 μM (Fig. 5f).

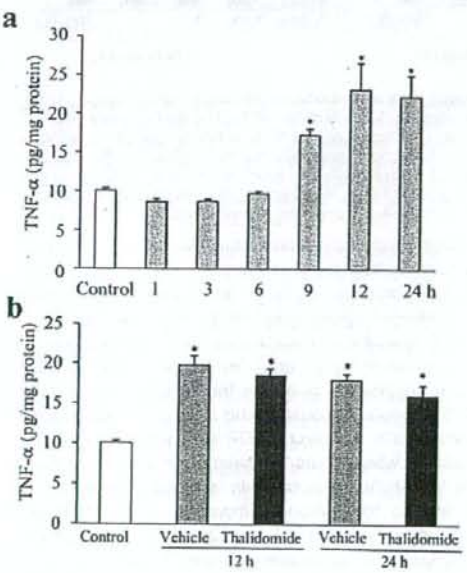

Fig. 4. Brain concentrations of TNF-α measured by ELISA. (a) Time course of changes in brain concentrations of TNF-α at 1–24 h after MCAO. (b) Effect of thalidomide at 20 mg/kg, i.p. (given three times) on TNF-α production at 12 and 24 h after MCAO. * $P<0.05$ vs. Control, $n=6–15$.

Effects of thalidomide on DPPH-induced free radicals

An inducer of stable free radicals, DPPH, was used to assess the radical-scavenging activities of thalidomide (which was extracted with ethanol) and trolox (1–100 μM) (a derivative of α-tocopherol; vitamin E). In ESR-spin trapping determinations, trolox (1–100 μM) reduced DPPH-induced free radical activity in a concentration-dependent manner. In contrast, thalidomide did not decrease DPPH-induced free radical activity, but trolox (10 μM) did (Fig. 6).

Effect of thalidomide on lipid peroxidation

The malondialdehyde (MDA) level in the supernatant from mouse forebrain homogenates increased after a 30 min incubation at 37 °C. The amounts of TBA substance (% of vehicle control) detected in the presence of thalidomide (0.1, 1, and 10 μM) were 95.2±2.3%, 94.9±1.4%, and 90.8±1.4%, respectively (each, $n=6$). The data show that thalidomide inhibited lipid peroxidation in a concentration-dependent manner, with a significant difference between the control and thalidomide-treated groups being detected at a concentration of 10 μM ($P<0.05$). Trolox at 100 μM significantly inhibited lipid peroxidation ($P<0.01$) (Table 2).

Anti-oxidative effect of thalidomide on focal ischemic brain in mouse

We examined the neuroprotective effects of thalidomide against MCAO-induced oxidative stress by performing immunohistochemical analysis for 8-OHdG, a marker of DNA damage, in the forebrain. No positive staining was detected in the sham group. At 24 h after MCAO treatment, however, strong 8-OHdG-immunoreactivity was detected in the penumbra area in the vehicle group (Fig. 7b, c). Thalidomide at 20 mg/kg, i.p. (given three times) significantly reduced the number of 8-OHdG-positive cells (Fig. 7b, c).

DISCUSSION

Neuroprotective effects of thalidomide

The main aim of this study was to investigate the neuroprotective effects of thalidomide. In a previous report, thalidomide reduced ischemic injury of the spinal cord in the rabbit (Lee et al., 2007), but as far as we are aware little is known about any effects of thalidomide against ischemic brain damage. We therefore investigated the neuroprotective effects of thalidomide in mice in which focal cerebral ischemia was produced by permanent MCAO, and we also explored its mechanism of action. We found that thalidomide displayed neuroprotective effects against histological injury in both the cortex and subcortex, and also against the neurological deficits evident after ischemia. When administered three times (at 10 min before, just before, and 1 h after MCAO), thalidomide reduced neuronal damage (infarct area and infarct volume) and functional damage (neurological deficit) at 24 h and 72 h after MCAO and at

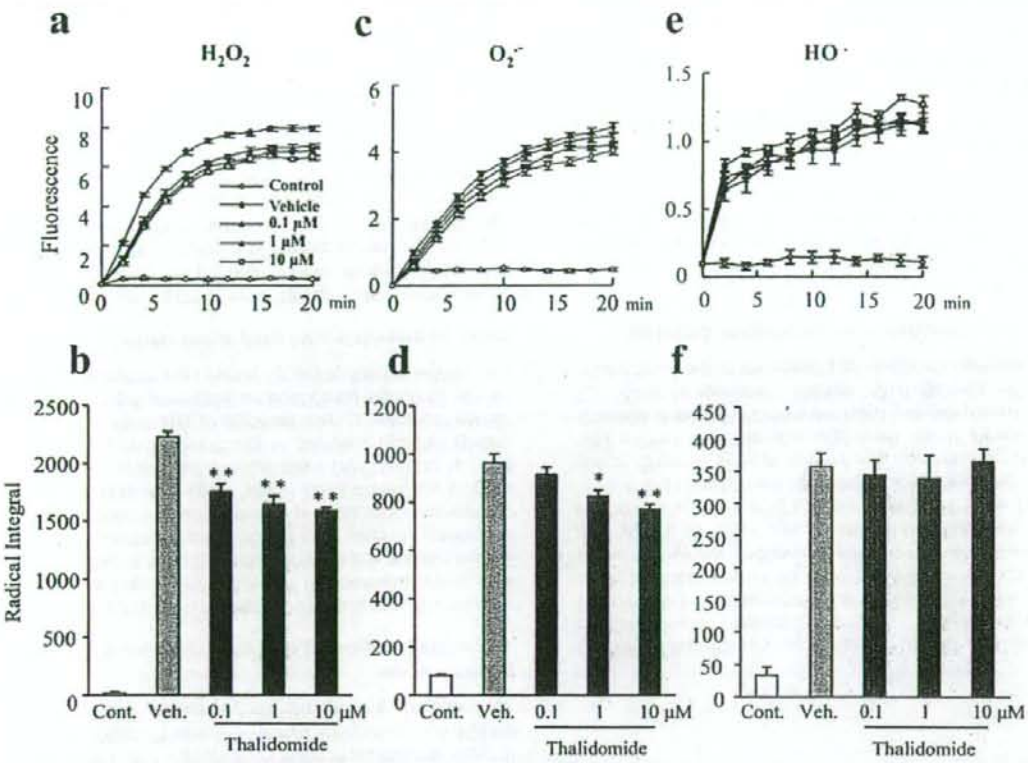

Fig. 5. Time-kinetic and concentration-response data for antioxidant activities of thalidomide against production of various radical species (H_2O_2, $O_2^{\cdot -}$, and · OH) in neuronal cells (RGC-5). (a, c, e) Cell cultures were treated with thalidomide (0.1, 1.0, or 10 μM) for 1 h, and then CM-H_2DCFDA at 10 μM (H_2O_2, $O_2^{\cdot -}$) or APF at 10 μM (· OH) was added for 20 min. ROS-production was stimulated with H_2O_2 at 1 mM, with KO_2 at 1 mM, or with H_2O_2 at 1 mM plus ferrous perchlorate (II) at 100 μM, and fluorescence was measured at various time-points. (a) The kinetics of DCFH oxidation by H_2O_2 in RGC-5. (c) The kinetics of DCFH oxidation by $O_2^{\cdot -}$ in RGC-5. (e) The kinetics of DCFH oxidation by HO·in RGC-5. (b, d, f) Integral of ROS production from the time-kinetics graph. Radical integral was calculated from (a, c, e), as described in "Experimental Procedures." Radical species were (b) H_2O_2, (d) $O_2^{\cdot -}$, and (f) · OH. Data are shown as mean±S.E., n=6. * P<0.05, ** P<0.01 vs. Vehicle-treatment alone.

72 h after MCAO, respectively. We additionally examined the effect of post-treatment of thalidomide. Thalidomide at 20 mg/kg was administered intraperitoneally at three times (at just after, 1 h after, 3 h after MCAO). In results, there were no significant changes in infarct volume between vehicle and thalidomide groups. The post-treatment of thalidomide only resulted in trace amounts reaching the brain because we used the MCAO permanent model, which limits vascular flow in the middle cerebral artery. Reportedly, post-treatment of thalidomide did not affect ischemic injury of spinal cord in rabbits, although pre-treatment prevented the injury (Lee et al., 2007). Therefore, our results were consistent with this previous report.

Involvement of angiogenesis

Vascular endothelial growth factor (VEGF) was expressed in the brain edema area after cerebral vein occlusion (Kimura et al., 2003). VEGF is an angiogenic factor that was first purified from the ascitic fluid of guinea pigs implanted with hepatocarcinoma cells (Senger et al., 1983) and induced by hypoxia (Schoch et al., 2002). Increases in VEGF were detected at 2 h after ischemia. Increased levels of VEGF were detected at 28 days after ischemia. The VEGF induction is most prominent in the cytoplasm of neurons (Hayashi et al., 1997; Marti et al., 2000). VEGF has been suggested as a new therapeutic mediator for ischemic diseases because of the angiogenic and neuroprotective effects. However, VEGF also increases vascular permeability, which could increase brain edema. Therefore, in the acute stage of brain ischemia, the effect of VEGF may be considered controversial. In our previous report, to investigate the anti-angiogenesis of thalidomide on tube formation by endothelial cells *in vitro*, HUVECs were co-cultured with fibroblasts in the presence of thalidomide. VEGF stimulated the formation of capillary-like structures by HUVECs, and thalidomide suppressed HUVEC tube formation in a concentration-dependent manner, its effects being significant at a concentration of

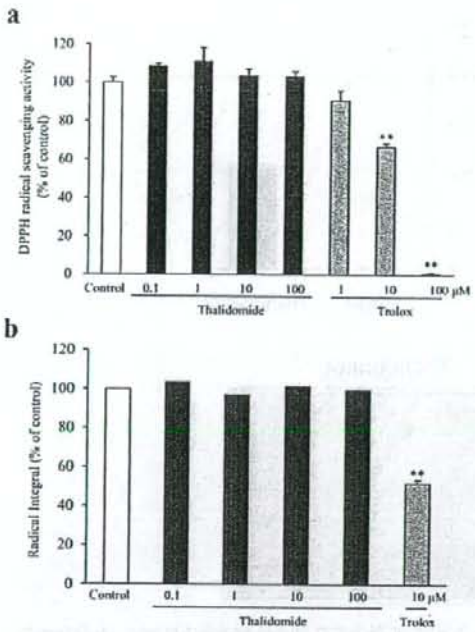

Fig. 6. (a) Hydroxyl radical-scavenging assay for thalidomide by the ESR spin-trapping method. (b) Effect of thalidomide on DPPH-induced free radicals (assessed by the method of Mellors and Tappel, 1966). Data are shown as mean±S.E., $n=3$. * $P<0.05$, ** $P<0.01$ vs. Vehicle-treatment.

100 μM (Yamamoto et al., 2008). In the present study, thalidomide at 0.1–10 μM inhibited the oxidation induced by radical species. In the present *vivo* study, we treated thalidomide at 20 mg/kg. Brain concentration of thalidomide (38 mg/kg) at 1.5 h after oral administration was 5.4 μM (Nicholls, 1966). It was suggested that an anti-angiogenesis effect of thalidomide needs higher concentrations (more than 100 μM) in brain, and the brain concentration estimated in our study was not reached to this concentration (100 μM). Taken together, the neuroprotective effect of thalidomide was detected at lower concentrations than anti-angiogenesis. Therefore, an anti-angiogenesis effect of thalidomide at 20 mg/kg, i.p. (in the present study) may not affect on its neuroprotective effects. We additionally examined the effect of thalidomide in a higher dose [50 mg/kg, i.p., three times (10 min before, just after and 1 h after MCAO)] on infarct volume, but there were no significant changes between vehicle and thalidomide groups. Thalidomide has anti-angiogenic effects based on inhibitory of VEGF. As mentioned above, a high dose of thalidomide at 50 mg/kg and more may aggravate the stroke outcomes by the effect of anti-angiogenesis.

Involvement of TNF-α

Next, we measured the brain concentrations of TNF-α by ELISA analysis. We found a significant increase in the TNF-α level in the brain as early as 9 h after MCAO, but there was no significant difference between the vehicle and thalidomide groups at either 12 or 24 h after MCAO (Fig. 4). One of the effects of thalidomide is known to be an inhibition of TNF-α, but in the present study such an effect was not observed in association with its effects against ischemic brain injury. In previous reports, depending on the type of cells stimulated with lipopolysaccharide (LPS) *in vitro*, thalidomide (used at concentrations that can be achieved *in vivo*) either enhanced or suppressed the synthesis of TNF-α (Miyachi et al., 1996; Shannon and Sandoval, 1996), suggesting that thalidomide can act as a regulator of the TNF-α level. Taken together TNF-α may not involve in the neuroprotective action of thalidomide in the present study.

Effect of thalidomide on oxidative stress

ROS such as H_2O_2, nitric oxide (NO), superoxide anion ($O_2 \cdot ^-$), and hydroxyl radical (OH) have been implicated in the regulation of many important cellular events, including transcription-factor activation (Schreck et al., 1991), gene expression (Lo and Cruz, 1995), and cellular proliferation (Murrell et al., 1990). However, excessive production of ROS causes events leading to death in several types of cells (Wolfe et al., 1994), and indeed ROS have been shown to induce death *in vitro* in cultured neurons (Ratan et al., 1994). It is known that cells possess antioxidant systems controlling the redox state, which is important for their survival, and H_2O_2 is often used to investigate the mechanism underlying ROS-induced cell death (Goldshmit et al., 2001). Since little is known about the anti-oxidative effects of thalidomide, we measured its radical-scavenging capacity in neuronal cells. We found that thalidomide significantly decreased the generation not only of H_2O_2, but also of $O_2 \cdot ^-$; indeed, our findings indicate that thalidomide has radical-scavenging capacity. We therefore examined the effect of thalidomide against MCAO-induced oxidative stress by performing immunohistochemical analysis for 8-OHdG. Oxidative stress is strongly related to the ischemic reperfusion model because after a reperfusion treatment, a great deal of ROS is produced. These ROS aggravate ischemic injury in brain. Therefore, the ischemic reperfusion model may be more appropriate than the per-

Table 2. Thiobarbituric acid reactive substance in mouse forebrain homogenates

Treatments	Concentration (μM)	% of control
Control		100
Thalidomide	0.1	95.2±2.34
	1	94.9±1.37
	10	90.8±1.40*
Trolox	100	38.6±1.04**

Thalidomide and trolox each reduced lipid peroxidation in mice forebrain homogenates.

* $P<0.05$ vs. control. Indicated values are expressed as mean±S.E., $n=6$.

** $P<0.01$ vs. control. Indicated values are expressed as mean±S.E., $n=6$.

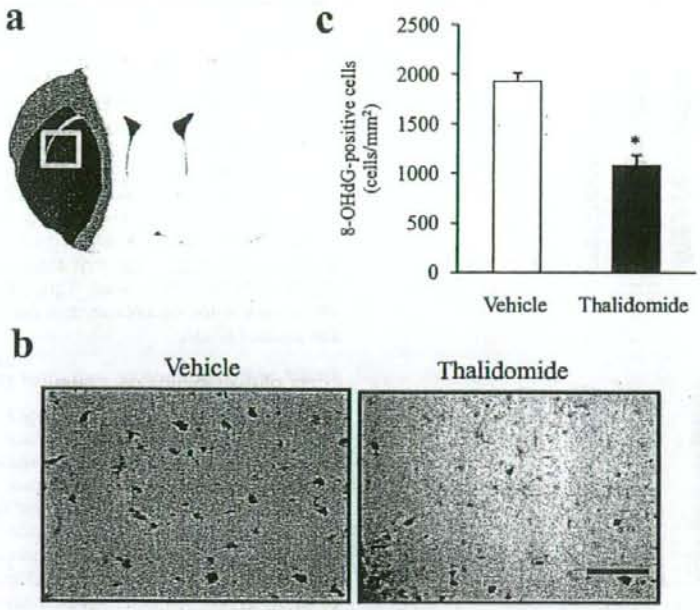

Fig. 7. Effect of thalidomide on MCAO-induced 8-OHdG-positive expression cells in brain at 24 h after MCAO treatment in mice. (a) Schematic drawing showing brain regions at 0.4–1.0 mm anterior to bregma (through the anterior commissure) (b) Thalidomide at 20 mg/kg, i.p. (given three times) reduced the number of TUNEL-positive cells (vs. vehicle treatment) in the ischemic penumbra area. (c) Quantitative representation of number of 8-OHdG-positive cells in ischemic brains treated with thalidomide or vehicle. * $P<0.05$ vs. Vehicle, $n=5$. Scale bar=25 μm.

manent model to examine the antioxidation of thalidomide in cerebral ischemia. However, in clinic, the permanent ischemic model is more similar to an actual clinical condition in human than the reperfusion model. Therefore, we examined this effect by using the permanent model in the present study. Our data indicate that it reduced the number of 8-OHdG-positive cells in both the ischemic core and penumbra areas. Furthermore, thalidomide inhibited lipid peroxidation in mouse forebrain homogenates in a concentration-related manner.

An antioxidation effect of thalidomide was not detected in the ESR assay or DPPH-induced free radical assay (Fig. 6). However, thalidomide had protective effects on lipid peroxidation and some radicals in the presence of cells (Fig. 5 and Table 2). In previous studies performed in the absence of microsomes, thalidomide had no effect on either microvessel formation or cell proliferation, suggesting that metabolites of thalidomide (4-OH-thalidomide, 3-OH-thalidomide, 3′-OH-thalidomide, 4′-OH-thalidomide, and/or 5′-OH-thalidomide) may be responsible for its anti-angiogenic effects (Bauer et al., 1998). Since in the present study an antioxidation effect of thalidomide was observed in the presence of cells, but not in their absence, the abovementioned metabolites of thalidomide may be responsible for its antioxidation effects as well as for its anti-angiogenic effects. However, further experiments will be needed to clarify the detailed mechanism(s).

Concentrations of thalidomide *in vitro* and *in vivo*

Recommended oral doses of thalidomide for the treatment AIDS and leprosy in adult human are 200–1200 mg/day, and by assuming an average body weight of 60 kg in human, we can estimate 3–20 mg/kg/day in animals. Therefore, we used 10 and 20 mg/kg as the experimental doses of thalidomide. The doses used in the present study were close to those in a previous study (Lee et al., 2007). Furthermore, after a single oral dose of 200 mg of thalidomide (as the US-approved capsule formulation) in healthy volunteers, the absorption was found to be slow and this resulted in a peak serum concentration (C_{max}) of 7.7 μM and in the present *in vitro* study, thalidomide at 1 and 10 μM showed antioxidation effects (Fig. 5). The concentrations of thalidomide were consistent with those of our *in vitro* effects. In a previous report, the concentration of [^{14}C]thalidomide in brain was 5.4 μM at 1.5 h after the oral administration of thalidomide in mice (Nicholls, 1966). The concentration was consistent with those of the present study *in vitro* (0.1–10 μM). It is suggested that when thalidomide at 20 mg/kg was administered intraperitoneally, thalidomide may reach enough concentrations to express pharmacological neuroprotection into brain.

CONCLUSION

In conclusion, thalidomide was found to reduce ischemic brain injury in mice subjected to permanent MCAO, and an

inhibitory action of thalidomide against oxidative stress may be partly responsible for its neuroprotective effects against such damage.

Acknowledgments—The authors thank Prof. Shinichi Kondo (Pharmaceutical Physical Chemistry, Gifu Pharmaceutical University) for technical support.

REFERENCES

Adom KK, Liu RH (2005) Rapid peroxyl radical scavenging capacity (PSC) assay for assessing both hydrophilic and lipophilic antioxidants. J Agric Food Chem 53:6572–6580.

Aydogan S, Turkcuoglu P, Celiker U, Ilhan N (2007) Effect of thalidomide on endostatin levels in retinal ischemia/reperfusion injury. Ophthalmologica 221:418–420.

Bauer KS, Dixon SC, Figg WD (1998) Inhibition of angiogenesis by thalidomide requires metabolic activation, which is species-dependent. Biochem Pharmacol 55:1827–1834.

Chan JY, Kwong M, Lo M, Emerson R, Kuypers FA (2001) Reduced oxidative-stress response in red blood cells from p45NFE2-deficient mice. Blood 97:2151–2158.

Flamm ES, Demopoulos HB, Seligman ML, Poser RG, Ransohoff J (1978) Free radicals in cerebral ischemia. Stroke 9:445–447.

Goldshmit Y, Erlich S, Pinkas-Kramarski R (2001) Neuregulin rescues PC12-ErbB4 cells from cell death induced by H(2)O(2). Regulation of reactive oxygen species levels by phosphatidylinositol 3-kinase. J Biol Chem 276:46379–46385.

Hara H, Friedlander RM, Gagliardini V, Ayata C, Fink K, Huang Z, Shimizu-Sasamata M, Yuan J, Moskowitz MA (1997) Inhibition of interleukin 1beta converting enzyme family proteases reduces ischemic and excitotoxic neuronal damage. Proc Natl Acad Sci U S A 94:2007–2012.

Hara H, Huang PL, Panahian N, Fishman MC, Moskowitz MA (1996) Reduced brain edema and infarction volume in mice lacking the neuronal isoform of nitric oxide synthase after transient MCA occlusion. J Cereb Blood Flow Metab 16:605–611.

Hara H, Kogure K (1990) Prevention of hippocampus neuronal damage in ischemic gerbils by a novel lipid peroxidation inhibitor (quinazoline derivative). J Pharmacol Exp Ther 255:906–913.

Hara H, Sukamoto T, Kogure K (1993) Mechanism and pathogenesis of ischemia-induced neuronal damage. Prog Neurobiol 40:645–670.

Hayashi T, Abe K, Suzuki H, Itoyama Y (1997) Rapid induction of vascular endothelial growth factor gene expression after transient middle cerebral artery occlusion in rats. Stroke 28:2039–2044.

Kimura R, Nakase H, Sakaki T, Taoka T, Tsuji T (2003) Vasogenic edema and VEGF expression in a rat two-vein occlusion model. Acta Neurochir Suppl 86:213–217.

Klausner JD, Freedman VH, Kaplan G (1996) Thalidomide as an anti-TNF-alpha inhibitor: implications for clinical use. Clin Immunol Immunopathol 81:219–223.

Krishnamoorthy RR, Agarwal P, Prasanna G, Vopat K, Lambert W, Sheedlo HJ, Pang IH, Shade D, Wordinger RJ, Yorio T, Clark AF, Agarwal N (2001) Characterization of a transformed rat retinal ganglion cell line. Brain Res Mol Brain Res 86:1–12.

Lee CJ, Kim KW, Lee HM, Nahm FS, Lim YJ, Park JH, Kim CS (2007) The effect of thalidomide on spinal cord ischemia/reperfusion injury in a rabbit model. Spinal Cord 45:149–157.

Lo YY, Cruz TF (1995) Involvement of reactive oxygen species in cytokine and growth factor induction of c-fos expression in chondrocytes. J Biol Chem 270:11727–11730.

Marti HJ, Bernaudin M, Bellail A, Schoch H, Euler M, Petit E, Risau W (2000) Hypoxia-induced vascular endothelial growth factor expression precedes neovascularization after cerebral ischemia. Am J Pathol 156:965–976.

Mellors A, Tappel AL (1966) Quinones and quinols as inhibitors of lipid peroxidation. Lipids 1:282–284.

Miyachi H, Azuma A, Hioki E, Iwasaki S, Kobayashi Y, Hashimoto Y (1996) Cell type-/inducer-specific bidirectional regulation by thalidomide and phenylphthalimides of tumor necrosis factor-alpha production and its enantio-dependence. Biochem Biophys Res Commun 226:439–444.

Moreira AL, Sampaio EP, Zmuidzinas A, Frindt P, Smith KA, Kaplan G (1993) Thalidomide exerts its inhibitory action on tumor necrosis factor alpha by enhancing mRNA degradation. J Exp Med 177: 1675–1680.

Murrell GA, Francis MJ, Bromley L (1990) Modulation of fibroblast proliferation by oxygen free radicals. Biochem J 265:659–665.

Nicholls PJ (1966) A note on the absorption and excretion of 14C-labelled thalidomide in pregnant mice. J Pharm Pharmacol 18:46–48.

Offner H, Subramanian S, Parker SM, Afentoulis ME, Vandenbark AA, Hurn PD (2006) Experimental stroke induces massive, rapid activation of the peripheral immune system. J Cereb Blood Flow Metab 26:654–665.

Paxinos G, Franklin KBJ (2001) The mouse brain in stereotaxic coordinates, 2nd ed. San Diego: Academic Press.

Ratan RR, Murphy TH, Baraban JM (1994) Oxidative stress induces apoptosis in embryonic cortical neurons. J Neurochem 62: 376–379.

Sampaio EP, Sarno EN, Galilly R, Cohn ZA, Kaplan G (1991) Thalidomide selectively inhibits tumor necrosis factor alpha production by stimulated human monocytes. J Exp Med 173:699–703.

Schoch HJ, Fischer S, Marti HH (2002) Hypoxia-induced vascular endothelial growth factor expression causes vascular leakage in the brain. Brain 125:2549–2557.

Schreck R, Rieber P, Baeuerle PA (1991) Reactive oxygen intermediates as apparently widely used messengers in the activation of the NF-kappa B transcription factor and HIV-1. EMBO J 10: 2247–2258.

Senger DR, Galli SJ, Dvorak AM, Perruzzi CA, Harvey VS, Dvorak HF (1983) Tumor cells secrete a vascular permeability factor that promotes accumulation of ascites fluid. Science 219:983–985.

Shannon EJ, Sandoval F (1996) Thalidomide can be either agonistic or antagonistic to LPS evoked synthesis of TNF-alpha by mononuclear cells. Immunopharmacol Immunotoxicol 18:59–72.

Toyoda K, Fujii K, Kamouchi M, Nakane H, Arihiro S, Okada Y, Ibayashi S, Iida M (2004) Free radical scavenger, edaravone, in stroke with internal carotid artery occlusion. J Neurol Sci 221: 11–17.

Wolfe JT, Ross D, Cohen GM (1994) A role for metals and free radicals in the induction of apoptosis in thymocytes. FEBS Lett 352:58–62.

Yamamoto T, Shibata N, Takashima M, Nakamura S, Toru T, Matsunaga N, Hara H (2008) Enzymatic resolution and evaluation of enantiomers of cis-5'-hydroxythalidomide. Org Biomol Chem 6:1540–1543.

(Accepted 16 December 2008)
(Available online 1 January 2009)

Neuroscience Letters 452 (2009) 156–161

Contents lists available at ScienceDirect

Neuroscience Letters

journal homepage: www.elsevier.com/locate/neulet

Cilostazol protects against hemorrhagic transformation in mice transient focal cerebral ischemia-induced brain damage

Yuko Nonaka[a,b], Kazuhiro Tsuruma[a], Masamitsu Shimazawa[a], Shinichi Yoshimura[b], Toru Iwama[b], Hideaki Hara[a,*]

[a] Department of Biofunctional Evaluation, Molecular Pharmacology, Gifu Pharmaceutical University, 5-6-1 Mitahora-higashi, Gifu 502-8585, Japan
[b] Department of Neurosurgery, Gifu University Graduate School of Medicine, 1-1 Yanagido, Gifu 501-1194, Japan

ARTICLE INFO

Article history:
Received 16 December 2008
Received in revised form 5 January 2009
Accepted 16 January 2009

Keywords:
Cerebral ischemia
Hemorrhagic transformation
Phosphodiesterase 3 inhibitor
Stroke

ABSTRACT

Cilostazol, an antiplatelet drug used to treat intermittent claudication, has been reported to offer neuroprotection and endothelial protection in animals with ischemic brain injury. Here, we evaluated the protection afforded by cilostazol against ischemic brain injury and hemorrhagic transformation. Mice subjected to a 2-h filamental middle cerebral artery (MCA) occlusion were treated with cilostazol (10 mg/kg, intraperitoneally just after the occlusion) or with vehicle. Histological outcomes (infarct volume and hemorrhagic transformation) and Evans blue extravasation were assessed after reperfusion. Mean infarct volume, hemorrhagic transformation, and Evans blue extravasation were all significantly reduced in the cilostazol-treated group. Thus, cilostazol protected against ischemic brain injury and hemorrhagic transformation in mice subjected to transient focal cerebral ischemia.

Accumulating evidence suggests that for acute ischemic brain attack, thrombolytic therapy may be a useful clinical strategy. The clinical efficacy of treatment with recombinant tissue-plasminogen activator (rt-PA) within a few hours after the onset of the ischemic attack has been demonstrated by the National Institute of Neurological Disorders and Stroke rt-PA Stroke Study Group [19]. However, if there is a delay in its administration or in reperfusion, hemorrhagic transformation can occur, often with fatal results. Indeed, the restrictions on the use of thrombolytic therapy may include, for instance, the very short "window" for its administration after the onset of the attack. One of the factors causing hemorrhagic transformation may be a disruption of the blood–brain barrier (BBB), which consistent mainly of endothelium [2]. For this reason, the proper treatment for acute brain ischemia might include not only thrombolytic therapy, but also BBB protection.

Cilostazol, an antiplatelet drug used to treat intermittent claudication, increases the intracellular level of cyclic AMP by inhibiting its hydrolysis by type III phosphodiesterase. Its principal reported actions include inhibition of platelet aggregation [8,9], antithrombosis in feline cerebral ischemia, and vasodilation via an increased cyclic AMP level [18]. A characteristic feature of cilostazol is that it has weaker hemorrhagic side effects than other antiplatelet drugs, indeed, it does not increase the bleeding time [20]. Recently, it has been reported that cilostazol has a neuroprotective effect against ischemic brain injury [3,11], and this neuroprotective potential has been ascribed to (a) its anti-inflammatory and anti-apoptotic effects (mediated by a scavenging of hydroxyl radicals), (b) decreased formation of tumor necrosis factor-α, and (c) an inhibition of poly(ADP-ribose) polymerase activity [10,12,13]. We further reported that cilostazol afforded neuroprotection against the permanent, filamental MCA occlusion-mediated increases in metallothionein-1 and -2 [21]. In addition, increasing evidence indicates that cilostazol may offer endothelial protection via both an inhibition of lipopolysaccharide-induced apoptosis [7] and an inhibition of neutrophil adhesion to endothelial cells (through a down-regulation of the expressions of adhesion molecules) [14–16]. Since endothelium is one of the main constituents of BBB, cilostazol may afford not only endothelial protection, but also BBB protection.

The above suggests that cilostazol may not only be neuroprotective, but also protect against hemorrhagic transformation during the reperfusion after ischemia. By so doing, cilostazol may prolong the time window for thrombolytic therapy. The aim of this study was to assess whether reperfusion-induced hemorrhagic transformation is indeed suppressed by cilostazol in a mouse MCA occlusion/reperfusion model.

The experimental designs and all procedures were in accordance with the Animal Care Guidelines of the Animal Experimental Committee of Gifu Pharmaceutical University. Male ddY mice (body weight, 24–28 g; Japan SLC Ltd., Shizuoka, Japan) were housed at controlled room temperature (24.5–25.0 °C), with a 12/12-h

* Corresponding author. Tel.: +81 582 37 8596; fax: +81 582 37 8596.
E-mail address: hidehara@gifu-pu.ac.jp (H. Hara).

0304-3940/$ – see front matter © 2009 Elsevier Ireland Ltd. All rights reserved.
doi:10.1016/j.neulet.2009.01.039

light/dark cycle. Mouse food pellets and tap water were provided ad libitum.

Cilostazol {6-[4-(1-cyclohexy-1H-tetrazol-5-yl)butoxyl]-3,4-dihydro-2-(1H)-quinolinone} was kindly gifted by Otsuka Pharmaceutical Co. Ltd. (Tokushima, Japan). Mice assigned to the cilostazol group were treated by intraperitoneal (i.p.) injection of cilostazol at 10 mg/kg body weight only once [viz. immediately after the completion of middle cerebral artery (MCA) occlusion]. Mice assigned to the vehicle group received an i.p. injection of 0.5% carboxymethyl cellulose sodium salt (CMC) without cilostazol at a timing and volume similar to that used in the cilostazol group. The injection volume was adjusted to 8 ml/kg body weight in all experiments.

Mice were anesthetized with 2.0–2.5% isoflurane (Merck Hoei Co. Ltd., Osaka, Japan) in air (21% O_2) via a face mask (Soft Lander; Sin-ei Industry, Saitama, Japan). Focal cerebral ischemia was induced [using an 8-0 nylon monofilament (Ethicon, Somerville, NJ, USA) coated with silicone hardener mixture (Xantopren; Bayer Dental, Osaka, Japan)] via the internal carotid artery, as described by Hara et al. [5]. In all animals during surgery, the body temperature was maintained between 37.0 and 37.5 °C with the aid of a heating lamp and heating pad. Any mice with pulmonary insufficiency or subarachnoid hemorrhage at the craniotomy due to thread penetration of cerebral artery were excluded under blind to the animal groups.

Mice were tested for neurological deficits at 22 h after reperfusion by an observer (Y.N.) who was blind to the animal groups. Scoring was done using the following scale: 0, no observable neurological deficits; 1, failure to extend the right forepaw; 2, circling to the contralateral side; 3, loss of walking or righting reflex [5].

At 22 h after reperfusion, mice were given an overdose of pentobarbital sodium (Dainippon Sumitomo Pharma, Osaka, Japan) and then decapitated. The brain was cut (using a microslicer) into 2-mm-thick coronal block slices at preselected positions ±3 mm from bregma. These slices were immersed for 30 min in a 2% solution of 2,3,5-triphenyltetrazolium chloride (TTC) (Sigma–Aldrich Co., St. Louis, MO, USA) in normal saline at 37 °C, then fixed in 10% phosphate-buffered formalin at 4 °C. TTC reacts with intact mitochondrial respiratory enzymes to generate a bright red color that contrasts with the pale color of the infarction. The caudal face of each slice was photographed (COOLPIX 4500; Nikon, Tokyo, Japan). Then, the unstained areas of the total, cortical, and subcortical infarctions were measured using Image J (http://rsb.info.nih.gov/ij/download/), and the infarction volume was calculated as in a previous report [6]. The numbers of mice underwent this assessment were eleven in each group.

For evaluating BBB permeability, Evans blue (Sigma–Aldrich, USA) dye extravasation was used, as described by Qin et al. [17]. At the time of reperfusion, 2% Evans blue in normal saline (4 ml/kg body weight) was injected into the jugular vein and allowed to circulate for 2 h. Mice were deeply anesthetized with pentobarbital sodium and transcardially perfused with saline until colorless fluid was obtained from the right atrium. Brains were quickly removed, and the hemispheres separated and weighed. Then, the right and left hemispheres were separately homogenized in 1 ml 50% trichloroacetic acid. The supernatant obtained by centrifugation was and diluted four-fold with ethanol. The samples were kept at 4 °C for 30 min, then, centrifuged for 30 min at 1000 × g. The amount of Evans blue dye was measured by means of a microplate fluorescence reader (excitation 610 nm; Skan It RE for Varioskan Flash 2.4; Thermo Fisher Scientific, Waltham, MA, USA.) and quantified with the aid of a standard curve. A quantitative evaluation of Evans blue extravasation was made by comparing the hemisphere ipsilateral to the MCA occlusion with the contralateral one in each mouse for correction of Evans blue which remained in blood vessels. The numbers of mice underwent this assessment were 13 in each group.

For evaluation of hemorrhage transformation, coronal brain slices were taken (as described for the measurement of brain infarction) and fixed in 10% phosphate-buffered formalin (without any staining). The caudal face of each slice was photographed, and the number of the hemorrhagic spots >500 μm in diameter was counted (one spot being counted as one point) by an observer (Y.N.) who was masked as to the experimental protocol. The numbers of mice underwent this assessment were 11 in each group.

Data are presented as means ± S.E.M. Statistical comparisons were made using a Student's *t*-test or Mann–Whitney *U*-test (neurological deficit score and hemorrhagic score) or a Chi-square test (for analyzing the exclusion and mortality rates). $P<0.05$ was considered to indicate statistical significance.

Among our mice, the mortality and the exclusion (because of subarachnoid hemorrhage or pulmonary insufficiency) were each approximately 10% at 24 h after ischemia [in each group (vehicle or cilostazol), the actual figure was 9.1%]. There was no significant difference between the groups in either mortality rate or exclusion rate ($P>0.05$, Chi-square test).

The ischemic group showed apparent neurological deficits at 22 h after end of the ischemia, and the cilostazol group exhibiting significantly lower neurological deficit scores than the vehicle group (Fig. 1(B)).

There was ischemic brain damage (pale colored infarction) in the ventrolateral cortex and subcortex in each group at 22 h after the 2-h MCA occlusion (Fig. 1(A)). Cilostazol treatment led to a significant suppression of both infarct size and total infarct volume (34.7% reduction in total infarct volume versus vehicle) (Fig. 1(B) and (C)). Analyzing the lesion area as separate cortex and subcortex regions (Fig. 1(D)) revealed that cilostazol significantly reduced the infarction in the subcortex (44.6% reduction; $P<0.01$ vs. vehicle), and tended to reduce it in the cortex (29.0% reduction; $P=0.14$).

In each group, at 2 h after the 2-h MCA occlusion, the weight of the ischemic (left) cerebral hemisphere was greater than that of the contralateral (right) one. There was no significant difference in the weight of the ischemic hemisphere (expressed as a percentage of the weight of the contralateral one) between the vehicle and cilostazol groups (6.1 ± 1.9% and 5.9 ± 2.1% of the weight of the contralateral hemisphere, respectively; $P=0.94$; Fig. 2(C)). Measurement of the extent of the Evans blue extravasation in the ischemic hemisphere in the vehicle and cilostazol groups gave values of 2.28 ± 0.22 and 1.72 ± 0.08 μg/g wet-brain-tissue ($P<0.05$), respectively. The corresponding values for the contralateral hemisphere were 1.87 ± 0.15 and 1.77 ± 0.13 μg/g wet-brain-tissue ($P=0.63$), respectively. Thus, cilostazol effectively prevented Evans blue extravasation in the ischemic hemisphere (Fig. 2(D)).

Hemorrhagic transformations were observed in all animals at 22 h after the 2-h MCA occlusion as scarlet dot lesions (hemorrhagic spots) within the area of ischemic damage (Fig. 3(A)). No mice displayed hematoma, which would be a significant space-occupying effect. The hemorrhagic spots in the cilostazol group were, on the whole, paler and smaller than those in the vehicle group. The points score for hemorrhagic spots >500 μm in diameter was significantly smaller in the cilostazol group than in the vehicle group both for the entire hemisphere (63.8% reduction; $P<0.05$; Fig. 3(C)) and for the cortex, but not for the subcortex (Fig. 3(D) and (E)).

In this study, cilostazol largely prevented hemorrhagic transformation after transient MCA occlusion in mice. Thrombolytic therapy, such as administration of rt-PA, for acute ischemic brain attack may be a reasonable strategy, and indeed is supported by accumulating evidence [19], but delay in instituting such therapy may allow hemorrhagic transformation to occur, with potentially fatal results.